A Digital Flux Injector for NMR Superconducting Magnets— Results of Operation with Superconducting Insert Coils

by

Rocky D. Mai

Submitted to the Department of Mechanical Engineering
in partial fulfillment of the requirements for the degree of

Master of Science in Mechanical Engineering

at the

MASSACHUSETTS INSTITUTE OF TECHNOLOGY

February 2006

Author .....
Department of Mechanical Engineering
January 15, 2006

Certified by .....
Yukikazu Iwasa
Research Professor, Francis Bitter Magnet Laboratory, and Senior Lecturer, Department of Mechanical Engineering, MIT
Thesis Supervisor

Accepted by .....
Lallit Anand
Chairman, Department Committee on Graduate Students

A Digital Flux Injector for NMR Superconducting Magnets—Results of Operation with Superconducting Insert Coils

by

Rocky D. Mai

Submitted to the Department of Mechanical Engineering
on January 15, 2006, in partial fulfillment of the
requirements for the degree of
Master of Science in Mechanical Engineering

Abstract

It has been known for some time that high-temperature superconductors (HTS) are critical for the construction of NMR magnets generating 1 GHz and above. Such systems generally require an HTS insert to be placed in the inner high-field region of a low temperature superconducting (LTS) magnet. Among the problems in the presently available HTS technology are splice resistance and index dissipation, which make it essentially impossible for HTS to operate in persistent mode. Unless operated in driven mode with a very stable power supply, the HTS insert generally cannot achieve NMR-quality temporal stability. Another option, proposed by Iwasa, is by the use of a digital flux injector (DFI), which is a transformer type of device that can inject a quantified amount of magnetic flux into a "slightly" resistive magnet to compensate the energy dissipation over time.

Previous work at the Francis Bitter Magnet Laboratory (FBML) showed a prototype DFI operate successfully with an LTS insert magnet and demonstrated the basic concepts of this alternative approach. Based on the prototype, the first full-scale DFI has been designed, built and operated with an LTS insert magnet and an HTS insert magnet separately. The design process, operation procedure and experimental results are the main topics of discussion in this thesis.

Thesis Supervisor: Yukikazu Iwasa
Title: Research Professor, Francis Bitter Magnet Laboratory, and Senior Lecturer, Department of Mechanical Engineering, MIT

Acknowledgments

First and foremost, I would like to thank my thesis advisor, Dr. Yukikazu Iwasa for giving me this opportunity to work on the DFI project. Thanks for introducing me to the world of superconductivity, for guiding me past various hurdles throughout my work, and for being the very best example of a first-class researcher and engineer.

The creation of this thesis would be impossible without the generous help from every member in the lab, thanks for your constant willingness to lend a helping hand or an attentive ear whenever one is needed. In particular, I would like to thank research scientists Haigun Lee and Juan Bascuñán for generously sharing their research experience and giving me helpful advices time after time. Special thanks goes to post-doctorate associate Seung-yong Hahn who provided enormous help and encouragement throughout the project, thanks for being there during numerous discussions and troubleshooting moments, not to mention those late-night liquid helium experiments.

Finally, no words from the dictionary can describe my gratitude toward my family and friends. Thank you for everything.

This work was supported by the NIH National Center for Research Resources.

Contents

List of Figures

List of Tables

Chapter 1

Introduction

1.1 Superconductivity

What is superconductivity? According to the conventional definition, it is a phenomenon in an element, inter-metallic alloy, or compound when a complete loss of electrical resistivity occurs below a certain critical temperature. Heike Kamerlingh Onnes, a Dutch physicist, discovered superconductivity in mercury in 1911, after he became the first one to successfully liquefy helium in 1908. Now almost a century later, superconductivity has been discovered in many other materials and has had many important scientific applications. Fig.1-1 shows the time of discovery and critical temperatures (T_c) for some of these superconductors. Based on T_c, they can be classified as either low temperature superconductors ("LTS"– T_c is near 0 K) or high temperature superconductors ("HTS"– T_c is near or above 100 K). Also note in the figure the boiling temperatures of two common cryogens, liquid helium (4.2 K) and liquid nitrogen (77 K), which are used to keep the superconductors below their T_c. Since liquid helium is much more expensive than liquid nitrogen, one advantage that HTS material has over LTS material is the possibility of using liquid nitrogen as cryogen.

In addition to T_c, critical current density (J_c) and critical magnetic field (H_c) are two other parameters which determine whether the material will be superconducting. Fig.1-2 shows a typical plot of the critical surface of a material. Any point that represents

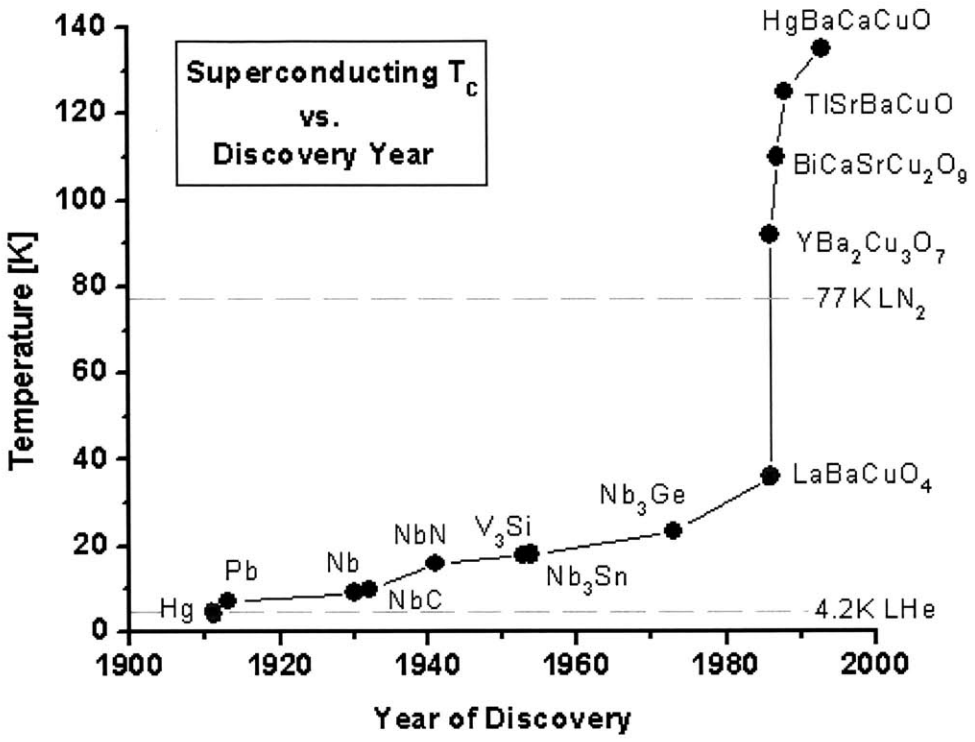

Figure 1-1 Discovery of superconductors and their critical temperature [1].

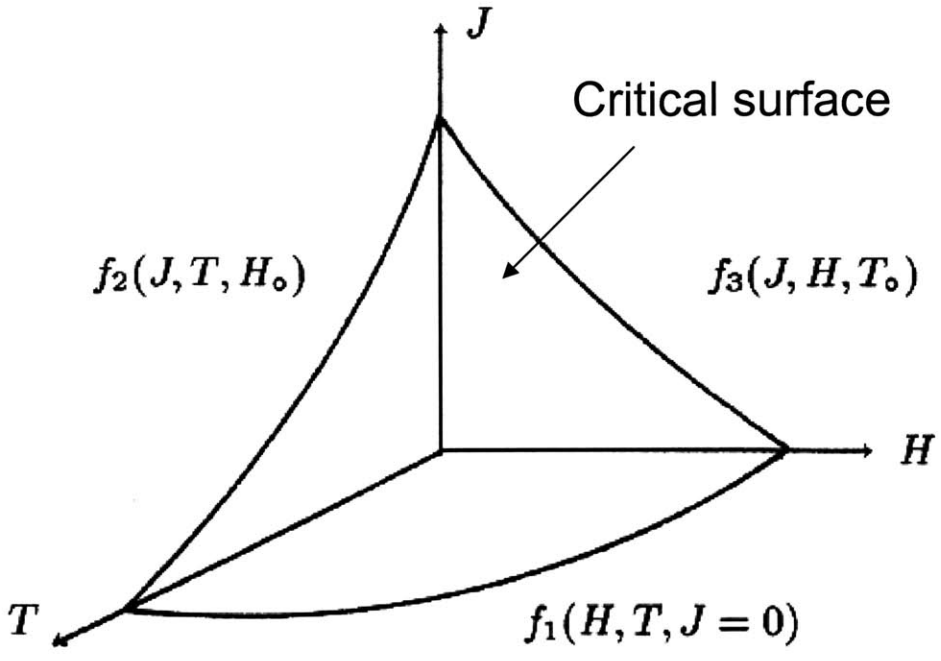

Figure 1-2 Critical surface of superconductivity [2].

a superconducting state of the material must lie on or below the critical surface. Therefore, the critical values essentially basically define the boundary of the material's "usefulness" as a superconductor. The higher the critical values, the more useful is the superconductor in applications. T_c and H_c are invariant thermodynamic properties of a material, on the other hand, it is possible to enhance J_c of a superconductor by means of metallurgical processing.

The obvious advantage of superconductors over normal conductors such as copper is that superconductors can conduct electricity with little or no resistance and associated energy loss, and therefore they can also transmit larger amounts of current compared with normal conductors of the same size. The electrical and magnetic behaviors of super-conductors and normal copper conductors are illustrated in Fig.1-3. Based on these behaviors, superconductors can be separated into two types. Type I superconductors, mainly metallic elements, have exactly zero resistance and energy loss; they are perfectly diamagnetic and they exhibit the so-called "Meissner effect" for which no magnetic field can penetrate inside the material except a very thin "penetration" layer at the surface. On the other hand, Type II superconductors are mainly inter-metallic alloys and oxide compounds, and they exhibit the "mixed state" due to isolated normal areas called "islands" which are the cause for energy dissipation during AC applications.

In DC applications, since current flows in the superconductor without resistance, once trapped in a closed loop, current can flow perpetually. Hence, a persistent magnetic field can be set up by a superconducting electromagnet provided that the circuit can be switched to a closed loop after current flows. Two widely used forms of electromagnets are solenoid and ring. For an ideal "long" solenoid coil with length $2b$, the magnetic field at the center of the coil is given by:

$$B_z(0,0) = \frac{\mu_o NI}{2b} \tag{1.1}$$

where $B_z(0,0)$ is the magnetic field density at the center, μ_o the magnetic permeability of free space ($4\pi \times 10^{-7}$ H/m), N the number of turns in the solenoid, and I the current. For a ring coil with diameter $2a$, on the other hand, the center field is given by:

$$B_z(0,0) = \frac{\mu_o NI}{2a} \tag{1.2}$$

As mentioned, the usefulness of a superconductor is determined by its critical values. Type I superconductors generally are not useful for magnet applications due to their low H_c values. In fact, until now, only a handful of Type II superconductors have earned the distinction of "magnet grade" superconductors for their useful and practical range of T_c, J_c, and H_c values [2]. These are NbTi and Nb_3Sn for LTS material, and BSCCO for HTS material. Several other potential "magnet grade" superconductors, such as MgB_2 and YBCO, are currently being investigated in research laboratories around the world.

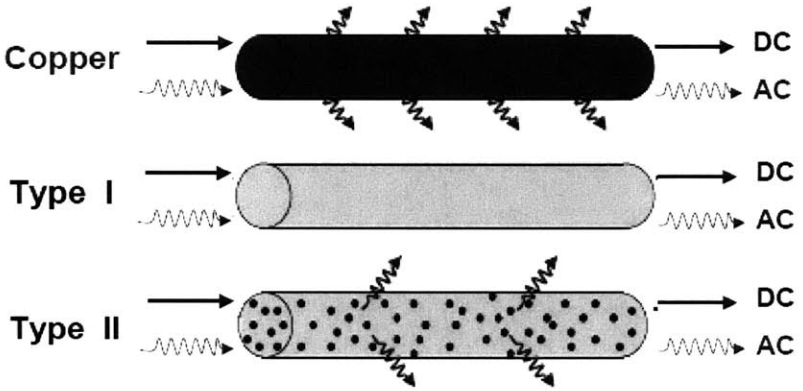

(a)

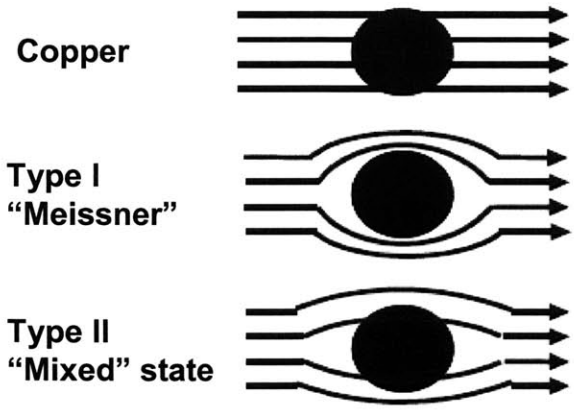

(b)

Figure 1-3 (a) Electrical behaviors, and (b) Magnetic behaviors for Type I, Type II superconductors and normal copper conductor respectively [3].

1.2 NMR Magnet

Superconducting magnets have important applications in many areas, such as magnetic levitations, particle accelerators, energy storage, fusion technology, NMR and MRI instruments. In these applications, superconducting magnets are used in place of copper magnets to eliminate issues long associated with electrical resistance, for instance, the problem of heating and the cost of electrical power to maintain long-term operation of these magnets. Here, we focus on superconducting NMR magnets.

NMR, or nuclear magnetic resonance, is a phenomenon which occurs when the nuclei of certain atoms are immersed in a static magnetic field and exposed to a second oscillating magnetic field [4]. NMR spectroscopy is the use of NMR phenomenon to study physical, chemical, and biological properties of matter. For instance, NMR spectroscopy is widely used by chemists to study chemical structure of molecules. Fig.1-4 shows a picture of the 920 MHz—one of the highest resolution—NMR magnet produced by Japan Superconductivity Technology, Inc. (JASTEC) in 2001. The center field of this magnet is 21.6 tesla, which is more than 400,000 times the magnetic field on the surface of Earth (0.5 gauss). Fig.1-5 shows a schematic cross-sectional view of the 920-MHz JASTEC NMR Magnet, which is wound with LTS superconductors. Submerged in superfluid helium (1.8 K), an outside magnet made of NbTi and an inside magnet made of $(Nb,Ti)_3Sn$ combine to generate a strong magnetic field at the center, and then a set of correction shim coils outside the magnets adjusts the center field for spatial homogeneity across the volume of the NMR sample. The higher this center field, the higher the resonance frequency of the sample, which in turn means higher resolution for NMR measurement.

The maximum resolution attainable by an NMR magnet is limited by the H_c - J_c characteristics of the superconductor in the innermost section, where the superconductor is exposed to the highest field. Since J_c decreases with magnetic field, this limits how much current can flow without quenching the inner layer. The resolution of 1 GHz (equivalent to a center field of about 23.5 T) is considered to be approaching the maximum resolution attainable by any all-LTS NMR magnet. To go beyond 1 GHz in

1. Bath-Cooled: NMR Magnet

High-resolution 920 MHz NMR Magnet (Nb-Ti/Nb3Sn @1.8 K) at National Institute for Materials Science, Tsukuba

Center Field:	21.6 T
Drift rate:	<0.000235 gauss/h
	<10 Hz/h
RT bore:	54 mm
Height:	5.5 m
Weight:	17 ton
(including cryogen & anti-vibration stand)	
LHe refill interval:	>21 days
refill volume:	386 liters
LN2 refill interval:	>27 days
refill volume:	520 liters

Courtesy of Mamoru Hamada (Kobe Steel)

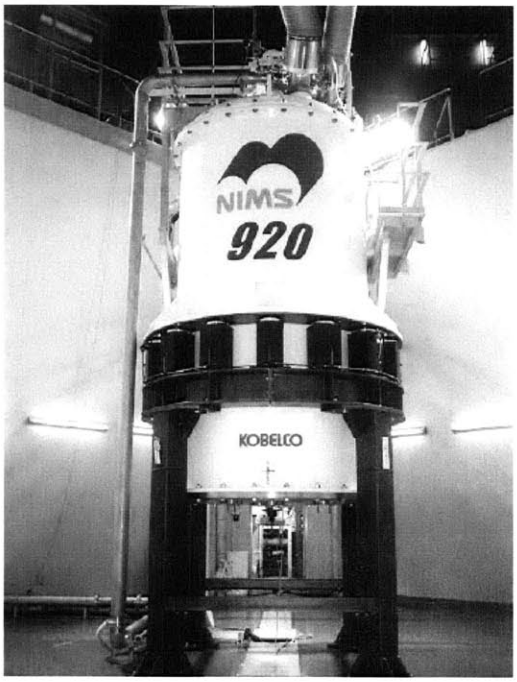

Figure 1-4 High-resolution 920 MHz NMR Magnet made by Japan Superconductivity Inc. (JASTEC) in 2001 [3].

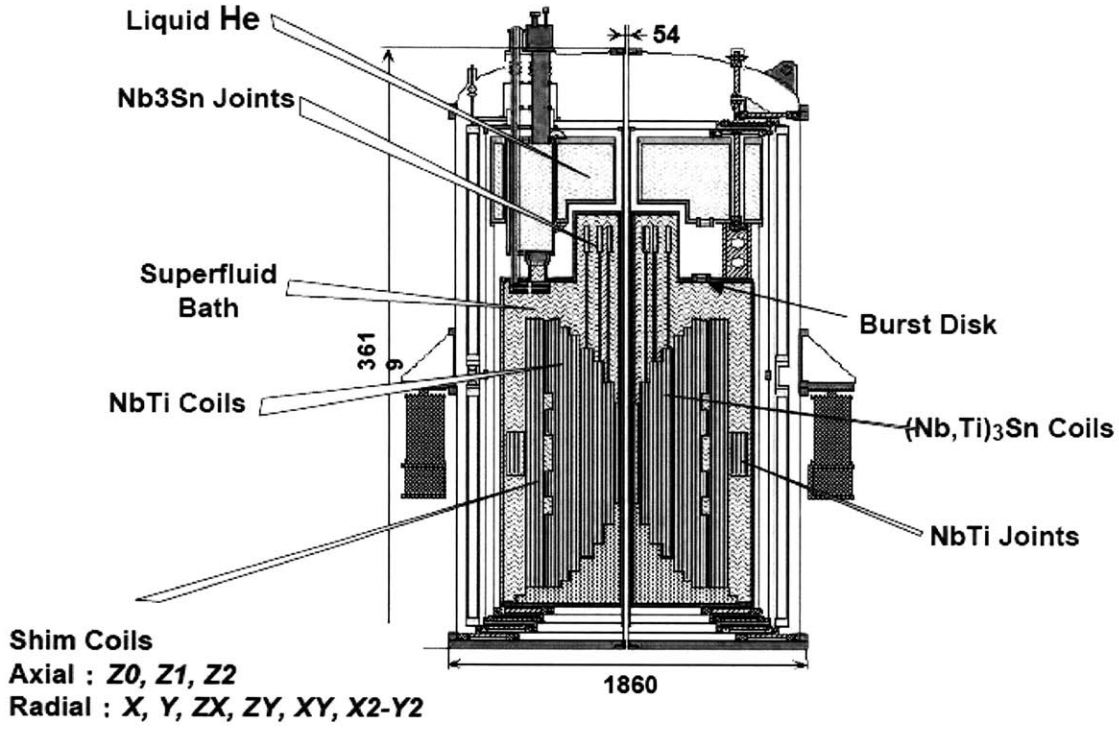

Figure 1-5 Cross-sectional view of the 920-MHz JASTEC NMR magnet [3].

future NMR, it is most likely that HTS materials, with their superior H_c-J_c properties, replace LTS materials at least for the innermost section of the magnet [5]. At the Francis Bitter Magnet Laboratory (FBML) in MIT, a three-phase project has been ongoing with the goal of building such a NMR magnet system with an HTS coil inside an LTS background magnet to achieve 1 GHz resolution. For each phase of the project, an HTS insert coil would be designed and made for operation inside an LTS background magnet.

1.3 HTS Insert Coil

Fig.1-6 shows a picture of the Phase 1, 50-MHz HTS insert magnet completed at MIT FBML in 2002 [6]. This insert magnet consists of 50 modules of double-pancake (DP) coils connected in series via 49 HTS-HTS splices. Each DP coil was wound with 45 m of three-ply BSCCO-2223/Ag tape with stainless steel reinforcement layer on each side. The overall resistance (R_{cir}) due to the HTS-HTS splices is 1.5 μΩ in liquid helium based on a previous measurement [6], and the total inductance of the insert (L_{mg}) is 1.12 H. The operating current of the insert (I_{op}) is 49 A, and the center field (B_{op}) during operation at this current level is 1.26 T. During the Phase 1 LTS/HTS NMR project, this HTS insert was coupled to an LTS background magnet to successfully produce an NMR frequency of 350 MHz [7]. The HTS insert was operated in driven mode by an external power supply, and the LTS background magnet was operated in persistent mode.

The differences between these two modes of operation are illustrated in Fig.1-7. In the driven mode, the magnet is permanently connected with an external power supply; there is no energy loss on the part of the superconducting magnet, but there is some loss on the part of the current leads connecting to the power supply. In the persistent mode, there is a persistent current switch (PCS) which can isolate the magnet totally from the external power supply once the magnet is charged up to its operating current. The PCS acts as an open during charge-up and acts as a short afterwards, and the operating current can remain constant in the magnet as long as the magnet is superconducting. Apparently, the persistent mode without the external power supply is the preferred mode of operation because of reduced cost of maintenance and better temporal field stability. In many cases, NMR magnets can stay in operation for years after the initial charge-up.

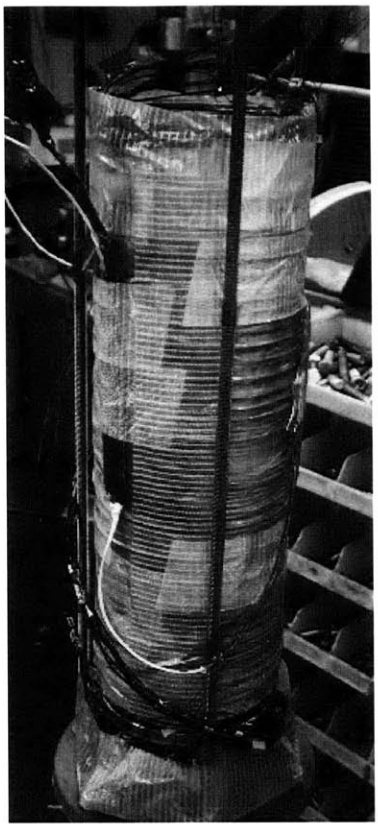

Phase I HTS Insert Coil

50 MHz, center field 1.26 T

BSCCO-2223/Ag tape

50 double pancakes (DP)

49 HTS/HTS splices

Operating current (4.2 K): 49.0 A

Splice resistance: 1.5 μΩ

Total inductance: 1.12 H

Inner diameter: 78.2 mm

Outer diameter: 120.3 mm

Insert length: 327.6 mm

Figure 1-6 Phase 1 HTS insert coil made in FBML, MIT. The splice resistance of 1.5 μΩ is based on a measurement done in 2002. As we shall see in Chapter 4, the actual circuit resistance has turned out to be considerably greater than 1.5 μΩ.

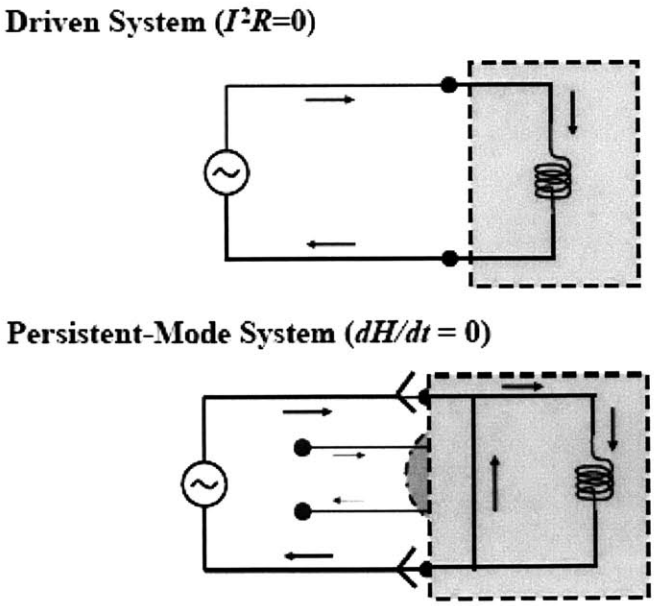

Figure 1-7 Driven system vs. persistent-mode system [3].

While LTS magnets are commonly operated in persistent mode, there are at least two problems which prevent the HTS counterparts to be persistent: 1) the resistance of non-superconducting HTS-HTS splices and 2) the resistance due to index dissipation.

The total length of the superconducting wire or tape in an NMR magnet is on the order of kilometers, therefore it is usually impossible to wind the coil with a single continuous piece of superconducting material, especially HTS material. Most coils consist of a number of layers or modules, and electrical connections in between them have to be made in the form of splices or joints. While the technology of making truly superconducting joints for LTS materials has matured over the years so that resistivity is not a problem, similar technology for HTS materials has not yet emerged. Presently, the most common method of making an HTS-HTS splice—via a "lap joint"—introduces resistance due to various solder and contact problems. Also, due to the brittle nature of HTS materials, even the slightest mishandling can damage the splice. The resistance of a good splice is the order of one nano-ohm in liquid helium, whereas the resistance of a bad one can be as high as micro-ohms.

The second problem of index dissipation is related to a material's non-ideal transition to the superconducting state, and it happens to have a more adverse affect on HTS materials than LTS materials. Ideally, as long as the current density in a superconductor is kept below J_c, the material would remain superconducting and have no resistance; as soon as the current density exceeds J_c, the superconductor would "quench" and become normal. However, real transition of a material between its normal and superconducting states actually takes place across a range of current densities, and this transition is characterized by the material's index number, n. Fig.1-8 shows the transition plots for three different cases: ideal, LTS and HTS. For the ideal case ($n = \infty$), there is a sharp transition at J_c: the material is superconducting for all values below J_c, during which no energy is dissipated and zero electric field is generated. The transition for LTS materials, which have typical index values in the range of 50 to 100, is very close to the ideal case, the electric field dropping quickly to zero for current densities below J_c. HTS materials—index number in the range of 10 to 20—have a more gradual transition, and significant electric fields can be generated even for current densities below J_c.

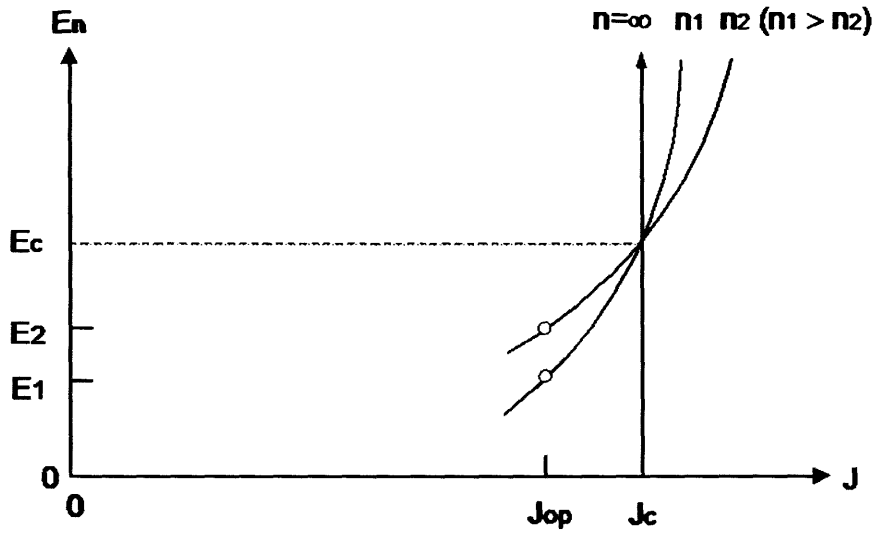

Figure 1-8 Electric field vs. current density for different index numbers [2].

The transition plots can be described by the following expression for index voltage:

$$V_n = E_n l = E_c l \left(\frac{I_{op}}{I_c} \right)^n = V_c \left(\frac{I_{op}}{I_c} \right)^n \tag{1.3}$$

The index voltage, V_n, which is equal to the index electric field, E_n multiplied by the length of the superconductor, is a power function of the ratio between the operating current (I_{op}) and the critical current (I_c). E_c, the critical electric field criterion used to establish J_c of a material, is generally set at 1 μV/cm. Since the operating current ratio is always less than unity, higher index number means lower index voltage and dissipation, that is why LTS magnets can be operated essentially in persistent mode.

The effect of the index dissipation in HTS material can be considered as additional resistance in the system. For a differential HTS material element, this resistance, R_n can be calculated as the derivative of the index voltage with respect to operating current:

$$R_n = \frac{V_c}{I_c} n \left(\frac{I_{op}}{I_c} \right)^{n-1} \tag{1.4}$$

The values of n and I_c also depend on the magnetic field that the material element is exposed to, and since the magnetic field in a magnet varies from location to location, the total effective resistance due to index dissipation must be evaluated as an integral over the entire volume of the magnet.

In the future, it can be reasonably expected that the splicing technology for HTS material will mature as in the LTS case and the resistance due to splices will become negligible. But in order to operate the HTS magnet in the preferred persistent mode, the problem of index dissipation will still have to be considered. It is for this consideration the idea of a digital flux injector was proposed.

1.4 Digital Flux Injector

Digital Flux Injector (DFI) was proposed by Iwasa as an alternative to the driven mode operation of an HTS insert coil. It enables the insert to effectively operate in persistent mode by periodically injecting an quantifiable amount of magnetic flux to compensate the dissipation in the insert. DFI is essentially a flux pump, and it consists of primary DP coils, secondary DP coils and superconducting switches all made from LTS Nb_3Sn tape with copper insulation on each side. One of the superconducting switches is connected in parallel to the secondary coil of the DFI and acts as a PCS for the HTS insert. A pair of lap joints connects the PCS with the HTS insert, and they can be BSCCO-Nb_3Sn or BSCCO-copper joints; in either case, the stainless steel layer of the BSCCO tape for the portion of the joint is peeled off before soldering.

Fig.1-9 shows the basic circuit diagram of the system. The primary and secondary coils are represented by self inductances L_p, L_s, and a mutual inductance M_{ps}. The LTS switches S_2 and S_3 are located in between the secondary coil and the HTS insert, which has a self inductance L_{mg} and an effective resistance R_{cir}. The primary coil of the DFI is connected by current leads to a power supply which generates the current pulses during flux injection, and the HTS insert is connected to an external magnet power supply for the initial charge-up of the operating current.

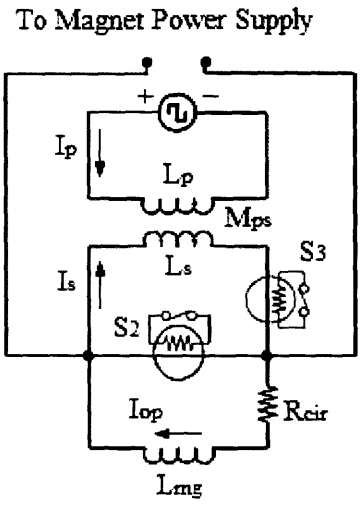

Figure 1-9 Circuit diagram of the DFI coupled to the insert coil.

The execution of the digital flux injection cycle has the following steps:

1. At the beginning of each cycle, switches S_2 and S_3 are closed and superconducting. The operating current I_{op}, which flows through the HTS insert and S_2, starts to decay due to resistance in the system;
2. Primary coil current I_p induces secondary coil current I_s such that $I_s > I_{op}$;
3. S_2 is heated up by a small current and becomes open circuit. I_{op} and I_s are forced to equilibrate, and the final current becomes $I_{op} + \Delta I_{op}$;
4. S_2 is switched closed, and the HTS insert is isolated from the secondary coil;
5. S_3 is heated and becomes open circuit. Current in the secondary coil is discharged;
6. I_p is reduced to zero and S_3 is switched closed, and the injection cycle is complete.

At the end of one injection cycle, the current in the HTS insert would increase by the amount of ΔI_{op} if there is no loss in the circuit. It is assumed that the directions of the current are the proper directions as shown in Fig.1-9 such that the magnetic fluxes of the secondary coil and the insert would add up during commutation. Otherwise, the flux injection would tend to decrease the current in the insert. If the operating current decay due to the resistance (R_{cir}) is also considered, then the amount of net increment would

be reduced, or there would not be any increment if the self decay rate is faster than the injection rate. An analytical expression for ΔI_{op} can be obtained in the following steps. First of all, the primary coil current I_p induces the secondary coil current I_s, which is given by:

$$I_s = \frac{M_{ps}}{L_s} I_p \tag{1.5}$$

During the current commutation, the total magnetic flux of the system is conserved:

$$L_{mg} I_{op} + L_s I_s = (L_{mg} + L_s)(I_{op} + |\Delta I_{op}|) \tag{1.6}$$

After substituting for I_s in (1.6), an expression for ΔI_{op} can be obtained as (1.7).

$$\Delta I_{op} = \frac{M_{ps} I_p - L_s I_{op}}{L_{mg} + L_s} \tag{1.7}$$

The goal of the flux injection cycles is to produce an ΔI_{op} larger than the self decay of the HTS insert. There are three phases to the DFI project and they directly follow the three phases of the 1 GHz LTS/HTS NMR project. In each phase, a new DFI unit would be built for the corresponding HTS insert coil. A schematic drawing of the DFI installed to the Phase 1 LTS/HTS NMR system is shown in Fig.1-10. The physical dimensions of the DFI are constraint so that the unit would fit inside the Phase 1 system.

Since the start of the DFI project in 2004, the first full-scale DFI unit has been designed and built. The unit was initially tested with an LTS insert coil for performance calibration and then coupled with the dissipative Phase 1 HTS insert coil. The ability of the DFI to compensate losses, thereby enabling the effective persistent operation of the HTS insert, was investigated.

The remaining part of this thesis will discuss 1) the design and making of individual components 2) the experimental setup of the DFI system, and 3) the results of operation.

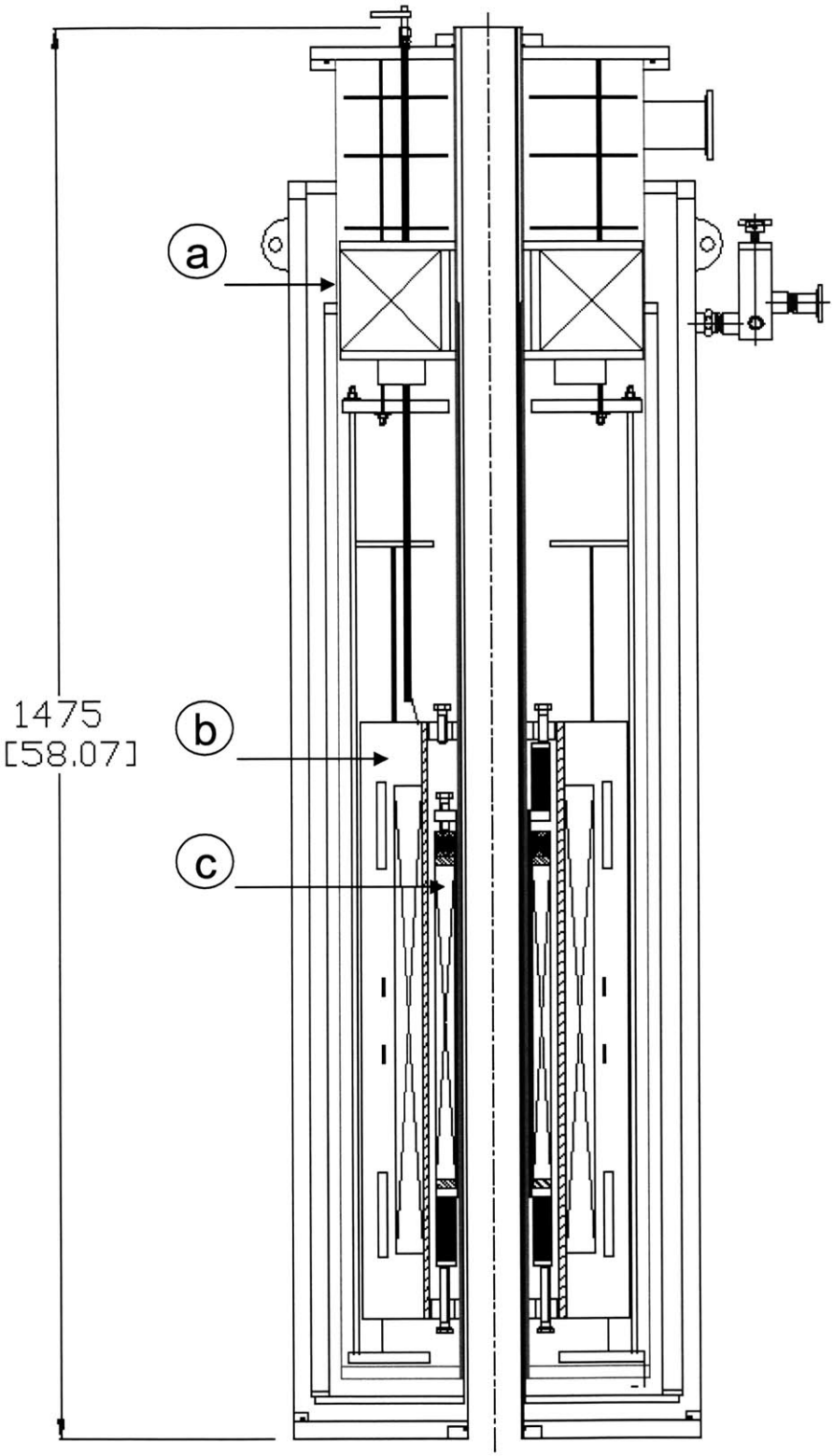

Figure 1-10 Schematics of the DFI+NMR system, illustrating the three components: a) DFI, b) LTS background magnet, and c) HTS insert coil. The overall height is 1475 mm.

Chapter 2

Design and Making

2.1 Basic Features of the DFI

The design of the first full-scale DFI was largely based on the prototype and most of the essential features remained the same [8, 9, 10]. There are three major components: the primary coil, the secondary coil, and the superconducting switches. The primary and the secondary coils have self inductances of L_p and L_s, and a mutual inductance of M_{ps}. Each coil consists of four double pancakes (DP) made of LTS superconducting tape. With a width of 3.1 mm and a thickness of 0.4 mm, the LTS tape contains Nb_3Sn superconductor sandwiched between two layers of copper 50 μm thick, and wrapped with "Nomex" insulation on the outside. The critical temperature of the tape, 18 K, is above the expected operating temperature of the DFI which is near the boiling temperature of helium (4.2 K). Also, the critical current and critical field values of the tape are much higher than the expected operating conditions of the DFI. Hence, the Nb_3Sn tape is an appropriate choice for making the primary and secondary coils of the DFI.

Fig.2-1 shows multi-view schematics of the basic DFI design. The four double pancakes of the primary and secondary coils were arranged 90 degrees apart and formed a toroid to minimize the magnetic field interference of the DFI on the NMR system. The DP coils of the primary coil were wound independently, each fixed to its own mechanical support. Then they were electrically connected in series by three LTS-LTS superconducting splices, and the two open ends were finally connected to the current

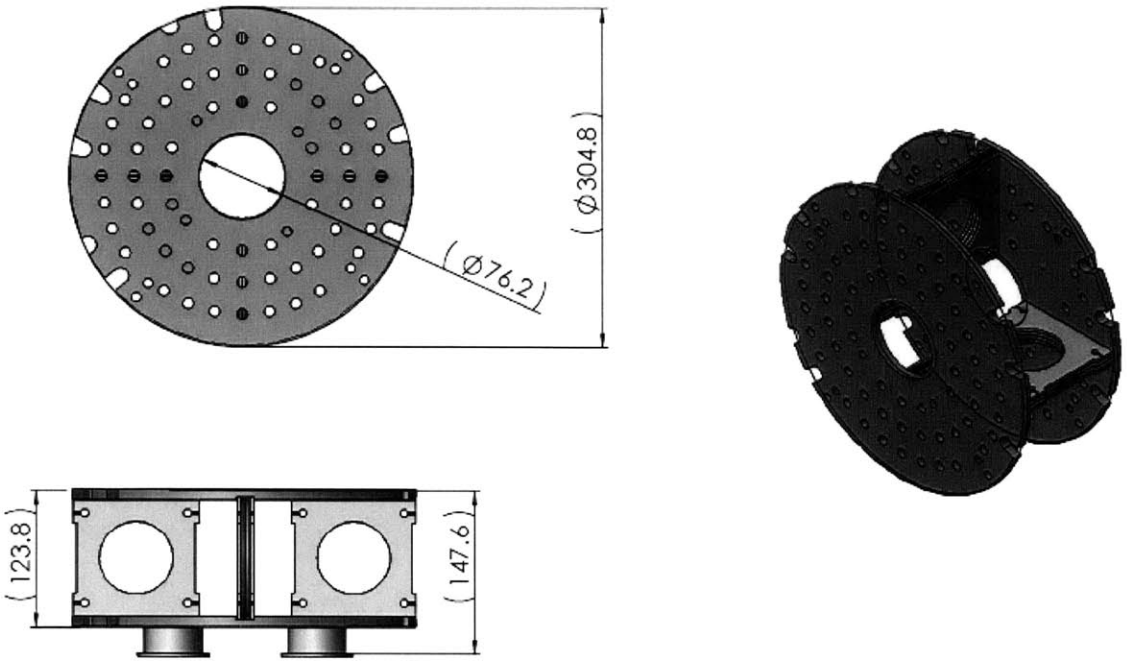

Figure 2-1 Multi-view drawings of the DFI design. Dimensions are in mm.

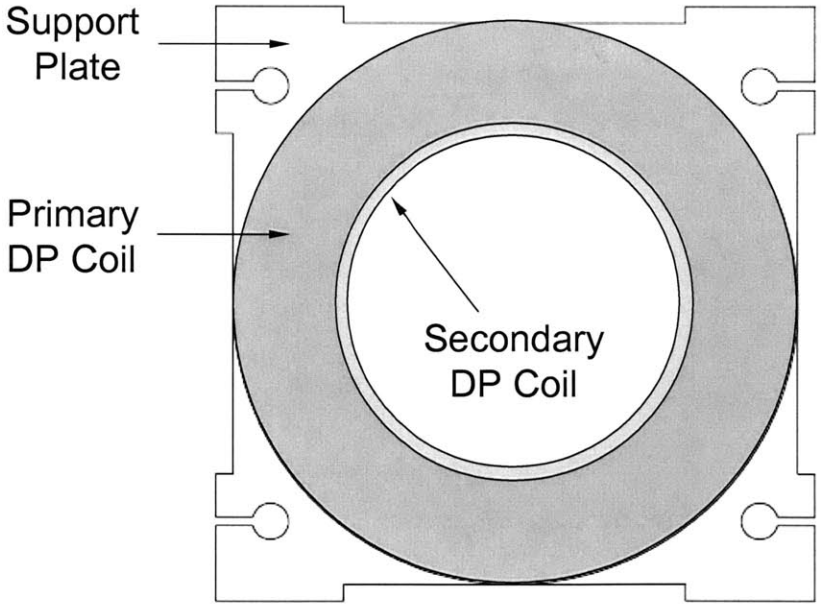

Figure 2-2 Schematics of the primary and secondary double-pancake (DP) coils.

leads of an external power supply. On the other hand, all DPs of the secondary coil were wound from one continuous piece of LTS tape, a feat possible due to the small number of turns for the secondary coil design. For magnetic coupling, each secondary DP coil was placed concentrically within a primary DP coil, as illustrated in Fig.2-2. The dimensions of the DP windings were designed so that the secondary DP coil would fit snugly inside the primary DP coil. Superglue was applied to further secure the secondary DP coil in place.

Located at the bottom of the DFI are two superconducting switches, S_2 and S_3, and they were made from the two free ends of the LTS superconducting tape of the secondary coil. Stainless steel strips were wrapped around the LTS tape to act as resistive heaters. As current passes through the stainless steel, the switch portion of the LTS tape would heat up and become nonsuperconducting, thereby creating an open circuit. After the heating current is shut off, the switch, which is constantly being cooled by the effluent helium vapor, returns to the superconducting state. During the operation of the DFI, S_2 and S_3 were turned on and off periodically to enable flux injection into the insert magnet.

While the prototype was previously built and operated on a test magnet simply to demonstrate the flux injection concept, the full-scale DFI was designed for operation with the Phase 1 HTS insert coil to make it effectively persistent. Hence, there were two major additional considerations during the design of the full-scale DFI: 1) the ability of the unit to compensate losses in the HTS insert, and 2) the constraints on the unit's physical dimensions imposed by the Phase 1 LTS/HTS NMR system.

2.2 Design Parameters

The physical dimensions of the primary and secondary double pancakes were considered to be the most important design parameters of the DFI, because not only do they affect the overall dimensions of the unit, they also determine the DFI's flux injection capability. The configuration of a DP coil is essentially determined by the inner diameter, the outer diameter and the number of turns in the winding. Once these values are known, the inductances of the primary and secondary coils can be calculated. Table 2.1 lists the values of some of these parameters for the full-scale DFI design in comparison with the

Table 2.1 Design parameters of the full-scale DFI vs. the prototype

Parameters	Primary Coil (Full-scale)	Secondary Coil (Full-scale)	Primary Coil (Prototype)	Secondary Coil (Prototype)
Toroid ϕ * [mm]	200		100	
DP inner ϕ [mm]	65.7	62.0	40.0	36.8
DP outer ϕ [mm]	104.8	64.1	67.8	38.2
Width [mm]	7.2	6.5	7.2	6.5
# Turns/DP	110	6	84	4
L [μH]	5400	17	2130	16
M_{ps} [μH]	169		73	
	Conductor: GE Nb_3Sn Tape (3.1 mm × 0.4 mm)			
Tape length/DP [m]	29.4	1.2	14.2	0.5

* Toroid diameter is the distance between the centers of opposite DPs

prototype. The toroid diameter, which is the diameter of the imaginary circle formed by the centers of the four DP coils, is an indicator of the overall size of the DFI unit. Note that the full-scale DFI is about twice in size than the prototype. As already mentioned, some of the physical dimensions of the full-scale DFI were constraint by the existing Phase 1 NMR system. In particular, the inner diameter of the DFI design had to be larger than 55 mm in order to accommodate a room-temperature bore in the Phase 1 cryostat used for NMR measurements. Meanwhile, the outer diameter had to be smaller than 300 mm in order to fit inside the same cryostat. The total height of the DFI unit was also constraint to be no more than 150 mm due to limited space available in the system. Therefore, the primary and the secondary DP coils would be designed within these constraints and reasonable machining tolerances in order to yield the optimal flux injection performance to compensate dissipations in the HTS insert.

It was assumed that the operating current flowing inside the dissipative HTS insert decays exponentially with a time constant of $\tau = L_{mg}/R_{cir}$, where L_{mg}, the measured inductance of the HTS insert is 1.12 H, and R_{cir}, the effective circuit resistance is 1.5 μΩ due chiefly to the total splice resistance from the 50 DPs in the HTS insert. Although there are other contributions to the circuit resistance from index dissipation and the joints between the PCS switch and HTS insert, they were not included in the design considerations because the operating current ratio was expected to be low and also the

resistance from the PCS joints was expected to be much less than 1.5 μΩ. The expected self decay rate of the operating current (I_{op}) in the insert could be obtained as (2.1).

$$\frac{dI_{op}}{dt} = -\frac{I_{op}(t)}{\tau} \tag{2.1}$$

In order to compensate for the self decay and to keep the operating current effectively persistent, DFI operation would need to induce a current increment in the insert, given by:

$$\Delta I_{op} = \left|\frac{dI_{op}}{dt}\right| t_{ip} = I_{op}\left(\frac{R_{cir}}{L_{mg}}\right) t_{ip} \tag{2.2}$$

Here ΔI_{op} is the required increment during a injection period of t_{ip} to keep up with the self decay. For instance, if the self decay rate of the operating current is 1 mA/s and the injection period is set as 10 seconds, then an increment of 10 mA per injection cycle is required.

To achieve the required current increment, the self inductances and mutual inductance of the primary and secondary coils were considered according to (1.7) given earlier.

$$\Delta I_{op} = \frac{M_{ps} I_p - L_s I_{op}}{L_{mg} + L_s} \tag{1.7}$$

While the self inductance of the insert L_{mg} and the operating current I_{op} have fixed values, the primary coil current I_p as well as the injection period could be varied during the operation, therefore the parameters needed to be considered were L_p, L_s and M_{ps}, which depend on the configurations of the primary and secondary DP coils, i.e. inner diameters, outer diameters, number of turns.

For design purposes, the primary coil input current was taken as 10 A, which could be supplied by one of laboratory power supplies, and the injection period was reasonably assumed to be 5 seconds considering the time necessary to operate the thermal switches. A number of possible configurations of the primary and secondary coils which conform

to the physical constraints previously mentioned were input to a computer program called SOLDESIGN (short for "solenoid design", and developed by Plasma Science and Fusion Center at MIT) to calculate the corresponding values of L_p, L_s and M_{ps}. Since these values were only calculated for one pair of primary and secondary DP coils, they were multiplied by four to account for the total of four DP pairs. The DP configuration which corresponds to a current increment larger than the required ΔI_{op} was then chosen as the final configuration.

Table 2.2 summarizes the major parameters for the DFI operation. The heater current of 2 A was chosen such that the switch temperature could quickly increase above T_c during current commutation. The minimum injection period achievable by the DFI also depends on the speed of the switch action. Finally, the measured inductance of the LTS insert is about the same as that of the HTS insert, therefore similar performance of the DFI could be expected during operation with the LTS insert, except there would be no self decay for the LTS case.

Table 2.2 Major parameters for the DFI operation

Toroid major diameter [mm]	200
# double pancakes	4
Primary coil inductance, L_p [μH]	5700
Secondary coil inductance, L_s [μH]	17
Mutual inductance, M_{ps} [μH]	169
Primary coil current, I_p [A]	10
Secondary coil current, I_s [A]	~100
Switch heater current, I_{sw} [A]	2
Injection period, t_{ip} [s]	5
LTS insert inductance [H]	0.98
LTS magnet constant [T/A]	0.021
HTS insert inductance [H]	1.12
HTS magnet constant [T/A]	0.0256

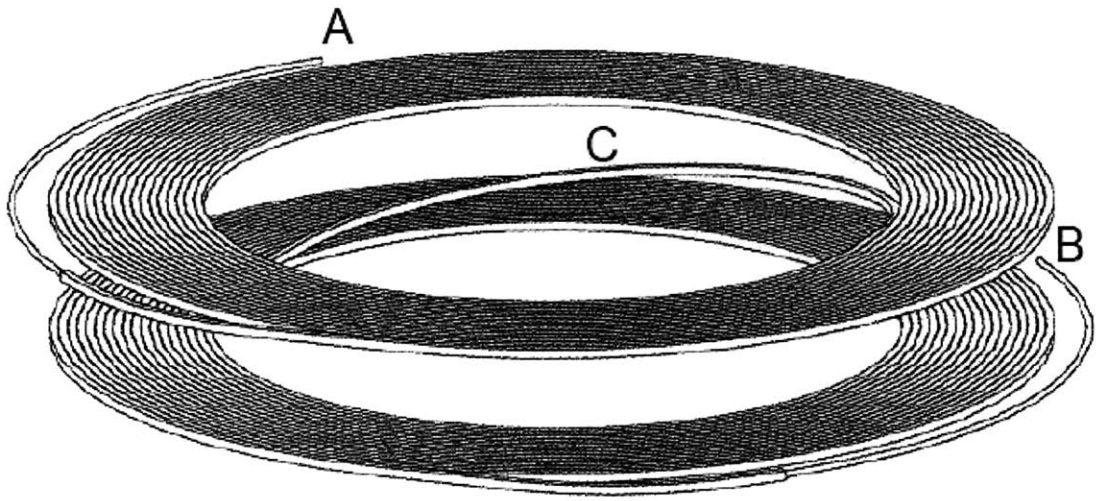

Figure 2-3 Schematic drawing of the double pancake coil. The winding starts from the center (point C) and finishes on the outside (points A and B).

2.3 Making of the Primary and Secondary Coils

Once the dimensions of the primary and secondary coils were determined, individual parts of the DFI support structure could be designed in SolidWorks. Three dimensional drawings of single parts and assemblies were created using the exact dimensions so that geometric compatibilities between parts could be checked, and afterwards the design drawings were sent to the machine shop for manufacturing.

The primary DP coils were made using a winding machine in the laboratory. As shown in the DP coil schematic in Fig.2-3, the winding process started in the middle at point C, the bottom half of the DP coil was wound first and then the top half. Upon finishing the winding, both open ends, points A and B, would end up on the outside, which would be very convenient for splice connection. The picture of a primary DP coil sandwiched in between supporting plates is shown in Fig.2-4. There are three insulated copper plates on both sides and in the middle of the winding, and then there are two G10 plates on the outside. The copper plates enable a uniform heat distribution within the winding and the G10 plates are mainly there to provide structure support.

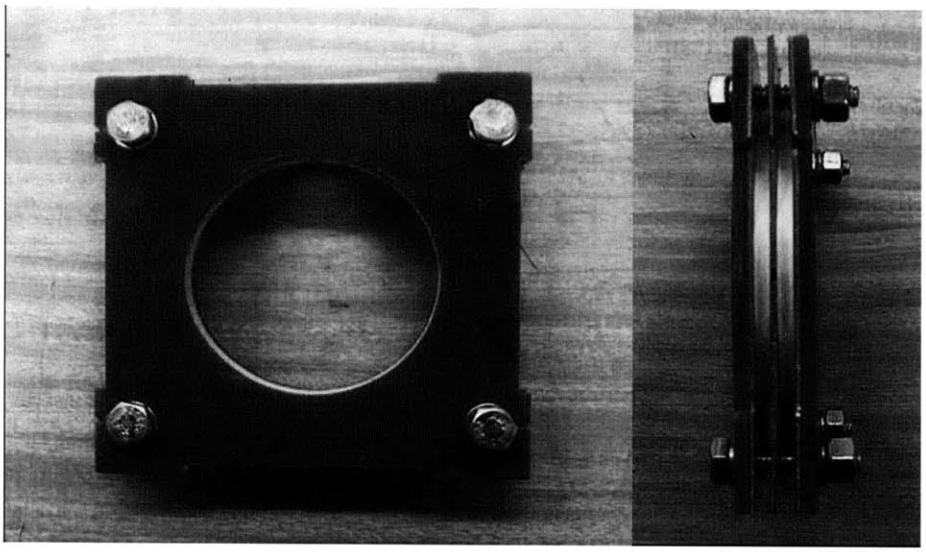

Figure 2-4 Primary DP coil and fixture.

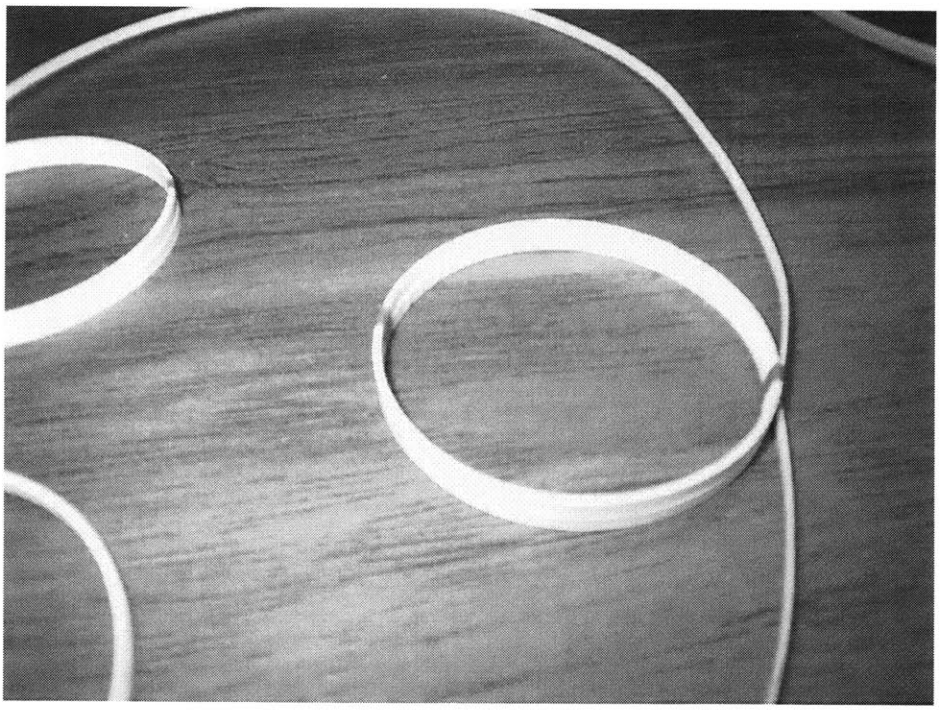

Figure 2-5 Secondary DP coils wound from a continuous piece of LTS tape.

As shown in Fig.2-5, the secondary DP coils were wound manually, with the help of fixtures machined to the exact inner diameter. This procedure avoided splices that would be otherwise required between the DP coils. With the secondary coil being part of the closed-loop circuit of the HTS insert, any mishandling of the unnecessary splices would have contributed to a larger effective circuit resistance, hence a faster self decay rate.

2.4 Making of the Switches

The design of the superconducting switch of the DFI is illustrated in Fig.2-6. The switch was made of several layers; from the outside to the inside, they are the following:

- Stycast epoxy
- Stainless steel heater
- Superconducting tape
- Stainless steel shim-stock
- G10 tubing

The Nomex insulation of the LTS tape was removed and the stainless steel strip was insulated with Kapton tape on both sides. Heating current were supplied to the stainless steel strip by external power supply through a pair of current leads. Voltage taps and thermocouples were placed inside the switch to monitor the response. Fig.2-7 shows a typical temperature response of the switch when tested in liquid nitrogen.

The temperature increase of the switch can be analyzed with a lump capacitance model assuming no significant temperature variation within the switch. From the energy equation, energy increase in the system is equal the difference between the heat input and the heat convection out of the system, as shown (2.3).

$$mc\frac{dT}{dt} = P - hA(T - T_{\infty}) \tag{2.3}$$

where m is the mass, c is the heat capacity, P is the heat input, h is the convective coefficient, A is the surface area, and T_{∞} is the ambient temperature, in this case 77 K. After substituting $\theta = T - T_{\infty}$, a differential equation for θ is obtained:

$$\frac{d\theta}{dt}+\frac{hA}{mc}\theta=\frac{P}{mc} \tag{2.4}$$

With the initial condition θ is zero at time zero, the following solution is obtained:

$$\theta=\theta_m(1-e^{-t/\tau_{sw}}) \tag{2.5}$$

where $\theta_m = P/hA$ is the equilibrium temperature difference and $\tau_{sw} = mc/hA$ is the time constant. In this case, if the system is considered to include the stainless steel heater, Kapton tape and Stycast epoxy, then $(mc)_{sys}$ of the system can be estimated as 0.6 J/K, and $(hA)_{sys}$ as 1 W/K. The heat input to the system is due to joule heating I^2R. When 1 A flows through a heater with a resistance 3 Ω, the heat input P is 3 W. For this heat input, the equilibrium temperature difference is 3 K, and the time constant is 0.6 second, which agrees very well with the temperature measurement in Fig.2-7.

When the switch is operated in liquid helium, the convective coefficient h becomes about 10 times smaller, and the heat capacity c also decreases with the decreasing temperature. Therefore, the equilibrium temperature difference could be 10 times higher while the time constant could remain pretty much the same.

During the DFI operation, the PCS switch becomes an open circuit to allow current commutation between the secondary coil and the insert magnet. Since the commutation process takes about one second to complete, this implies that the switch would need to remain above T_c for at least one second. Therefore the thermal response of the switch places a limit on the DFI's minimum injection period or maximum injection rate.

The switching action greatly affects the helium boil-off rate in the system and thereby limits the duration of the DFI operation unless helium is constantly refilled. For each watt of heat input, 1.4 liter of liquid helium evaporates every hour. During a typical DFI injection period of 5 seconds, 12 W of power goes into the switch for a total of 1 second, which means on average there are 2.4 W of heat input during the operation and 3.36 liters of liquid helium boil off every hour.

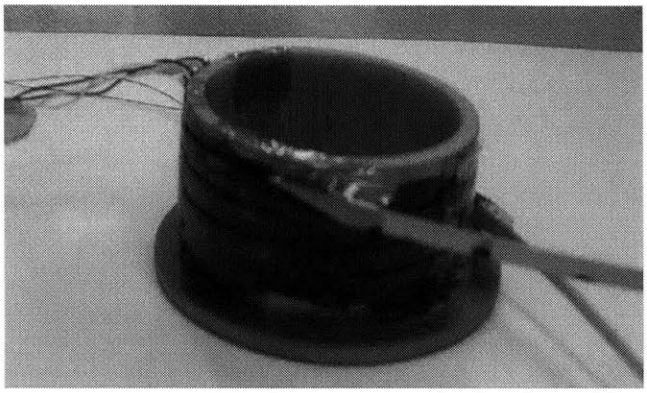

(a)

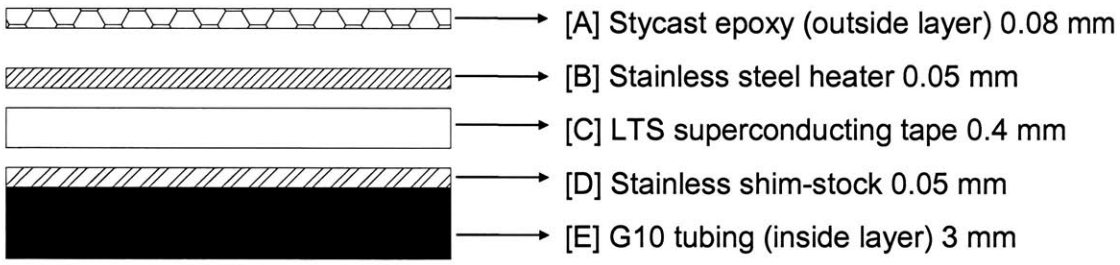

(b)

Figure 2-6 (a) Superconducting switch; (b) Design of the switch. The Nomex insulation of the LTS superconducting tape [C] is removed for better heat conduction; Kapton tapes are put on both sides of the stainless steel heater [B] for electrical insulation purpose. Dimensions are thicknesses.

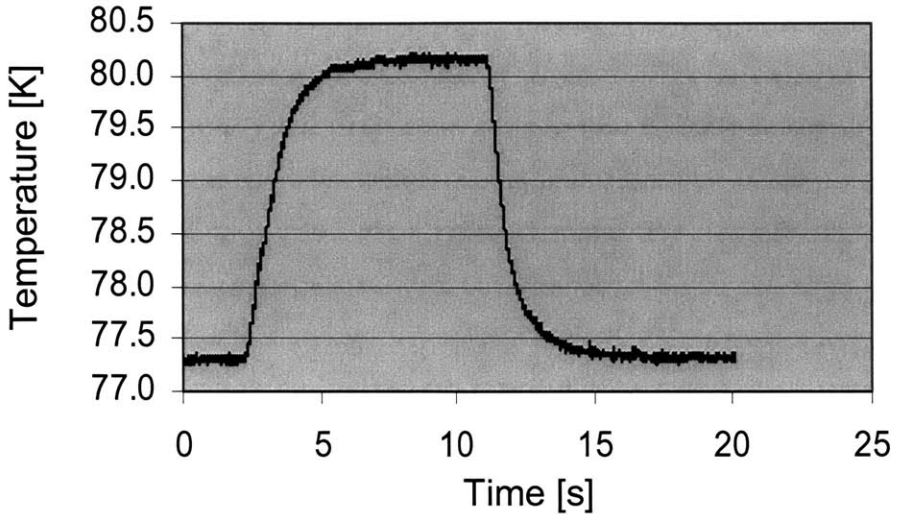

Figure 2-7 The temperature response of the switch to a heating current of 1 A in liquid nitrogen. The heating current is turned off at t = 12 s, and a maximum temperature rise of about 3 K is recorded by Chromel-gold thermocouples.

2.5 DFI Assembly

The primary and secondary DP coils and the thermal switches were assembled together. Figs.2-8 and 2-9 show photos of the DFI assembly. The top and bottom copper plates form the main support structure for the DFI assembly. Four grooves on each copper plate fix the positions of the primary DP coils 90 degrees apart in a toroid. Meanwhile, perforations on the plates contribute to additional surface areas for convective cooling by helium vapor; some of the holes are also necessary for clearance of the current leads, cryogen transfer lines and signal wires.

Both the DFI assembly and the insert magnet hang from the top flange of the cryostat. During operation, the insert magnet are submerged in liquid helium, whereas the DFI assembly is slightly above the helium level. The thermal switches of the DFI and the insert are soldered.

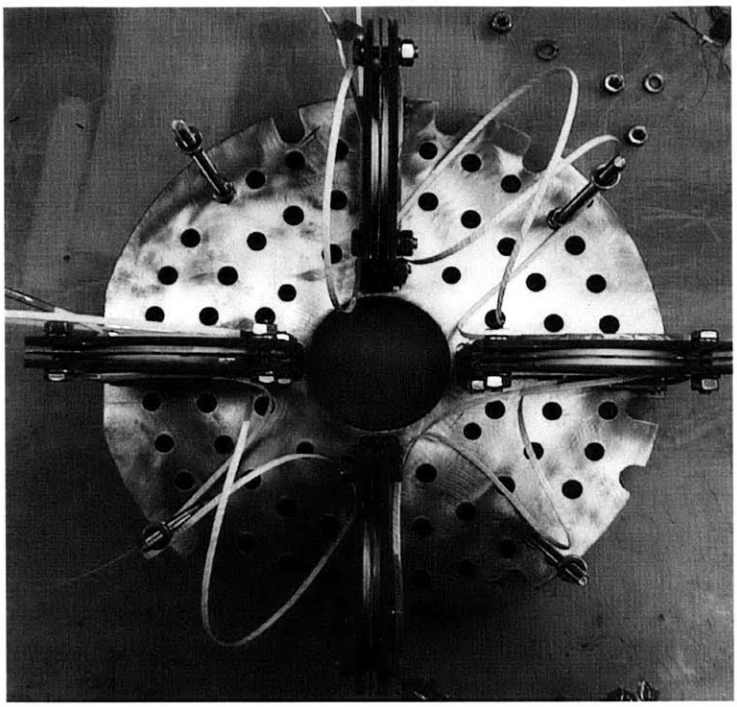

Figure 2-8 Assembly of the DFI. The four primary DP coils are arranged in a toroid and electrically connected in series by three LTS-LTS splices. The two open ends are then connected to an external power supply through a pair of current leads.

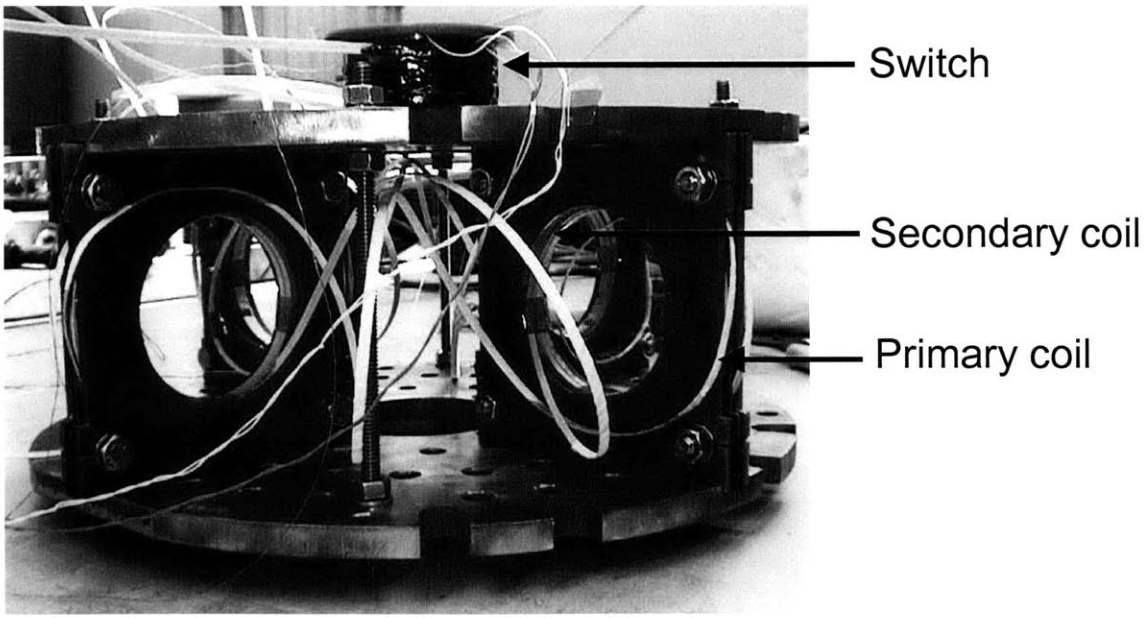

Figure 2-9 An upside-down view of the DFI system during assembly. The secondary coil DPs are secured snugly inside the primary DPs for magnetic coupling. The switches positioned at the bottom (shown here as top) of the DFI are cooled by vapor helium.

Chapter 3

Experimental Setup and Operation

3.1 Experimental Setup

After the DFI was designed, built and coupled with an insert magnet, it was put inside a cryostat so that experiments could be performed in liquid helium. Fig.3-1 shows the schematics of the DFI unit and the insert magnet inside a cryostat, while Fig.3-2 shows the picture of the actual system before it was put in the cryostat. The cylindrical wall of the cryostat is comprised of vacuum layers and a liquid nitrogen jacket in order to minimize the heat input into the system. As mentioned earlier, the DFI unit was first tested with an LTS insert coil to gauge various aspects of its performance. The LTS insert coil, as shown in Fig.3-2, has a self inductance of 0.98 H and a magnet constant of 0.021 T/A, which means a magnetic field of 0.021 T is generated at the center with 1 A flowing in the magnet. After the operation, the LTS insert coil would be removed from the DFI system and the Phase 1 HTS insert would be attached with DFI. The HTS insert magnet has a self inductance of 1.12 H, a magnet constant of 0.0256 T/A, and an estimated total resistance of 1.5 $\mu\Omega$.

Before the DFI/Insert system was put inside the cryostat, twisted pairs of signal wires were placed on various locations in the system in order to obtain measurement values. For instance, Chromel-Gold-0.07 at.% Iron thermocouples, initially calibrated in liquid helium, were used to measure the temperatures of the superconducting switches. The sensitivity of the thermocouple varies with temperature and for 30 K and below, it is

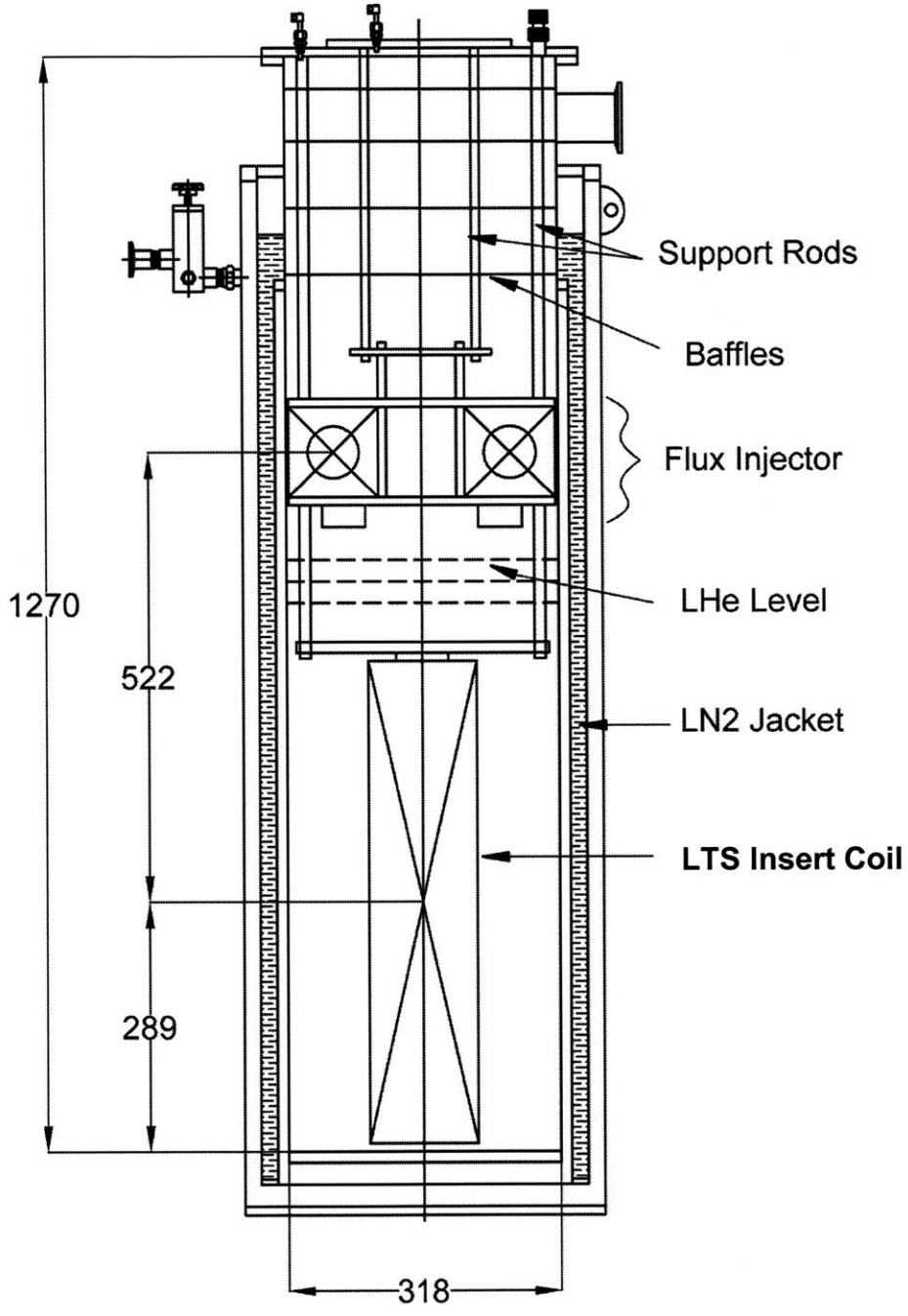

Figure 3-1 Schematics of the full-scale DFI coupled to the LTS insert coil. Dimensions are in mm.

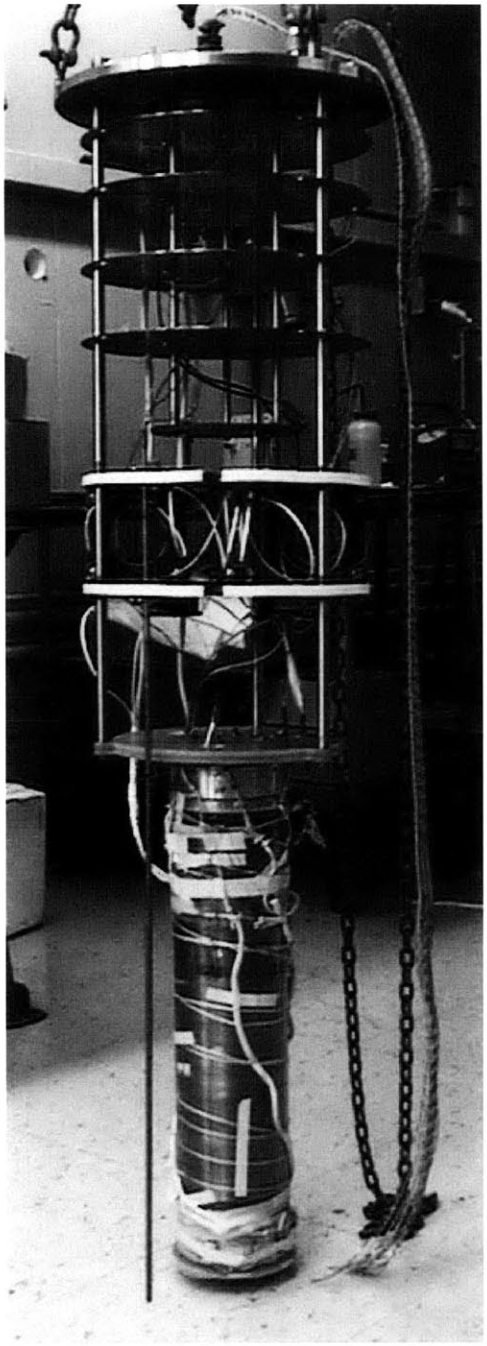

Figure 3-2 The actual DFI coupled to an LTS insert coil.

about 16 μV/K. The liquid helium level in the system was measured by a helium level sensor made of NbTi superconductor positioned alongside the DFI system. The magnetic field density at the center of the insert magnet was measured in several ways: by a search coil; hall sensors; and voltage measurement across the magnet. Various other voltage taps were necessary for measuring the resistance of joints and splices in the system. Finally, copper current leads were attached to the primary coil of the DFI and the insert magnet respectively.

The DFI was placed above the insert magnet so that the magnetic from the insert would not affect the performance of the DFI and vice versa. Another consideration was that the heat input to the switches would not be "dumped" directly into the liquid helium. Effective operation of the switches relies on convective cooling by the effluent helium vapor. At the beginning of the experiment, liquid helium was first filled up to just under the switches. During DFI operation, liquid helium was consumed and the level would drop until it reached a certain point where the effluent vapor could no longer provide sufficient cooling for the switches, and this happened when the level dropped below the G10 plate from which the insert magnet was hung. Below this level, either liquid helium has to be refilled or the DFI injection frequency has to be reduced in order for the switches to operate properly.

3.2 Data Acquisition System

Fig.3-3 shows the flowchart of the DFI experiment, which consists of the DFI system, the power supplies, the signal wires, and the LABVIEW system which controls the power supplies and acquires measurement data. Four power supplies were necessary in the experiment for the primary DP coil, the heaters of the superconducting switches, and the initial charge-up of the insert magnet. The power supply charging up the insert could be controlled manually and could be removed after the charge-up process. The other three power supplies were controlled through the back-panels by LABVIEW digital outputs in order to produce periodic current profiles necessary for the DFI operation. The actual current outputs of the power supplies were also measured using shunt resistors. The measurements of the DFI system, such as magnetic field, temperature and liquid helium

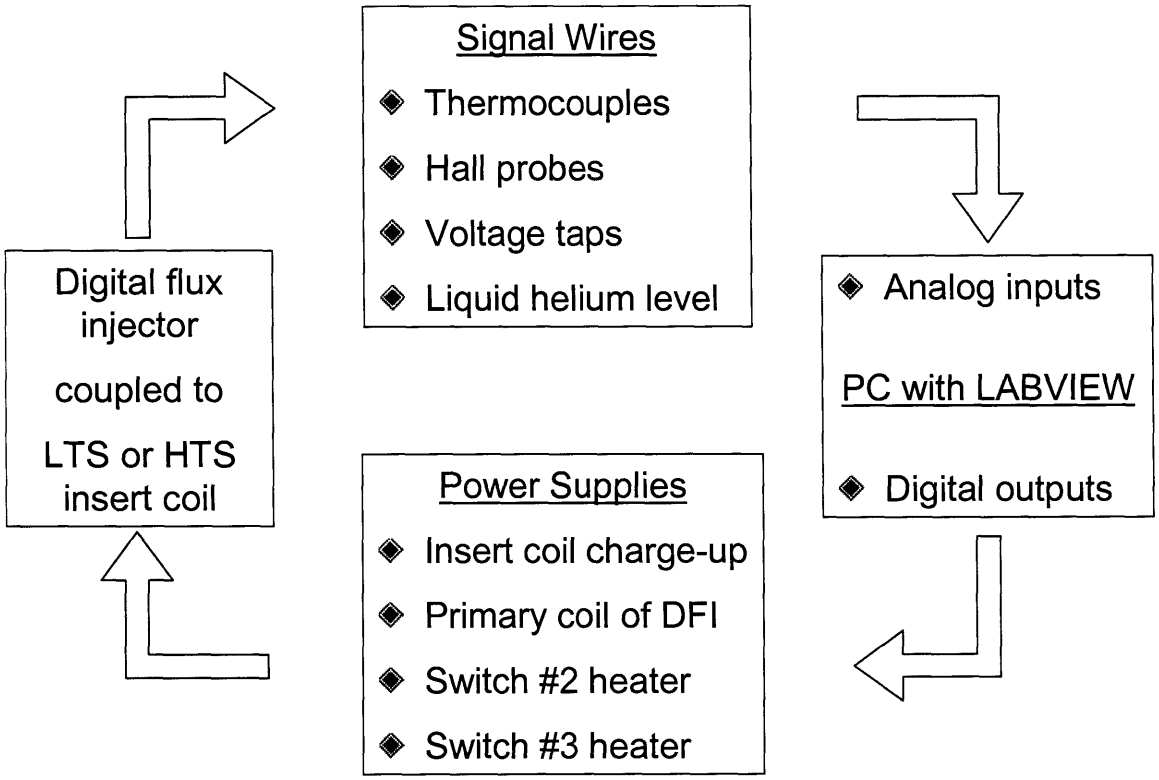

Figure 3-3 Components of the DFI experimental system including the LABVIEW acquisition system and software on a PC, external power supplies for the DFI and the insert magnet, the DFI and insert magnet system inside the cryostat, and various sensors and signal wires for measurement.

level were then acquired through the analog input channels of LABVIEW and stored in the computer. Various gains were used for the input channels depending on the expected magnitude of the signals, for example, signals from the thermocouple were on the order of 10 μV and thus a gain of 1000 was necessary to capture the signal. Sampling rates of the channels were set to 100 scans per second.

3.3 Operation of the DFI

Before the operation, liquid helium would first need to be transferred to the cryostat housing the DFI and the insert. The procedure to get the system ready for operation could be broken down into several steps. First of all, the integrity of the vacuum in the cryostat wall was checked. The night before the experiment, the entire system inside the cryostat was pre-cooled to 77 K with liquid nitrogen. The next morning, liquid nitrogen was purged out of the system using helium gas with a pressure of about 1000 torr at the beginning and 2000 torr near the end of the purge to make sure no nitrogen would remain in the cryostat. The system was then cooled from 77 K to 4.2 K using liquid helium with a driving pressure of no more than 50~100 torr; temperature inside the cryostat was closely monitored. Liquid helium would start collecting when temperature reached about 4.2 K and then slightly higher driving pressure could be used. Once the liquid helium level meter indicated that the liquid helium had reached just below the DFI switches (690 mm from the bottom of the cryostat), the transfer would stop, all transfer lines would be removed, and the insert magnet was ready for charge-up.

Since the DFI can inject magnetic flux into the insert, it is essentially charging up the magnet. Such charge-up test was performed with the LTS insert. Since the LTS insert was initially idle, there was no operating current. Equation (1.7) for current increment could be revised for this case while also taking into the consideration the fact that the secondary coil inductance, L_s is much smaller than the insert inductance, L_{mg}.

$$\Delta I_{op} = \frac{M_{ps} I_p}{L_{mg}} \tag{3.1}$$

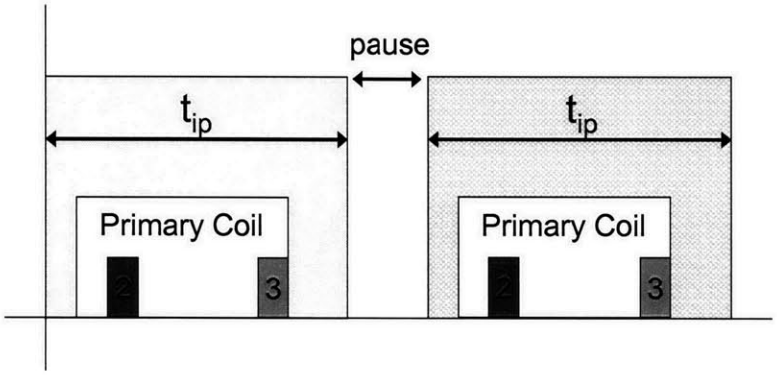

current profiles:

p/coil [0.5, 4.0 s]

sw2 [1.0, 1.5 s]

sw3 [3.5, 4.0 s]

p/coil current = 10 A

switch current = 2 A

switch time = 0.5 s

t_{ip} = 5 s; pause = 0

Figure 3-4 Typical current profiles for the primary coil ("p/coil") and the switch heaters ("sw2", "sw3") during DFI operation. The "switch time" is the duration during which a heater is turned on, and in this case, each heater is turned on for 0.5 s every cycle.

In fact, since L_s is about 10 times smaller than the mutual inductance, M_{ps}, (3.1) could be used as a good approximation for ΔI_{op} as long the operating current, I_{op} is small, i.e. $M_{ps} I_p \gg L_s I_{op}$.

During operation, digital pulses were sent from LABVIEW to the power supplies to produce current input pulses for the injection cycle, as illustrated in Fig.3-4. The current levels of 10 A for the primary coil and 2 A for the switch heaters were preset in the power supplies; only the on-and-off times would need to be determined. During a typical injection with a period of 5 seconds, the primary coil current is turned on at t = 0.5 s and induces the secondary coil current. At t = 1 s, heater current for switch S_2 is turned on to allow current commutation between the secondary coil and the insert magnet, as a result of which the insert current is incremented by ΔI_{op}. After that, switch S_2 is closed at t = 1.5 s and isolates the insert. Switch S_3 is heated at t = 3.5 s and becomes open circuit, and current in the secondary coil is discharged. Then, at t = 4 s, the primary coil current and the S_3 heater current are both turned off and the DFI returns to its initial state. The next injection cycle can follow immediately afterwards or after a pause.

For the HTS case, the insert magnet was first charged up to its operating current by an external power supply. Since the insert was connected to both superconducting switches, in order for the current to flow through the insert, both S_2 and S_3 were heated and non-superconducting during the charge-up period. Once the operating current (50 A) was reached, the heaters were turned off, and the switches cooled by vapor helium would return to the superconducting state. As a result, the operating current was trapped in the closed loop formed by the insert and the switch S_2. The self decay rate of the HTS insert could be obtained by magnetic field measurements at this point before turning on the DFI. Then, as DFI operation started, the effect of the flux injection could be observed.

3.4 Magnetic Field Measurements

Three independent methods were used to measure the magnetic field at the center of the insert, and from these measurements, the effect of the DFI operation could be obtained. The first method used the terminal voltage of the insert magnet, the second used the

output voltage of a search coil mounted inside the magnet bore, and the third used the output voltage of a hall sensor (Toshiba THS118) positioned at the center of the insert magnet. The results of all three measurement methods were compared with each others and with the theoretical value from circuit analysis.

3.4.1 Insert Magnet Voltage Measurement

When a steady current flows in the superconducting magnet, there is no voltage drop across the magnet because there is no resistance. But during DFI operation, as magnetic flux is injected into the system and current is incremented, an inductive voltage (V_{mg}) is set up across the magnet. Fig.3-5 shows a typical measurement of this inductive voltage and its numerical integration by MATLAB. Note that the voltage spikes are pretty much identical due to the stability of DFI system. The integrated voltage can be used to calculate the current increment, ΔI_{op} by the following relation:

$$\int V_{mg} dt = L_{mg} \Delta I_{op} \tag{3.2}$$

Since the magnetic constant of the insert magnet (either LTS or HTS) is known, ΔI_{op} can also be converted to ΔB_{op}, which is the magnetic flux increment.

3.4.2 Search Coil Voltage Measurement

The idea behind the search coil measurement is pretty much the same as the magnet voltage measurement, except the flux increment due to DFI operation is now detected by a copper solenoid located inside the insert magnet. The measurement of the search coil voltage and its integrated value can be used to obtain the magnitude of the flux increment as in the following:

$$\int V_{sc} dt = N_{sc} A_{sc} \Delta B_{op} \tag{3.3}$$

where N_{sc}, the total number of turns in the search coil is equal to 23540, and A_{sc}, the effective area for magnetic flux penetration, is equal to 1.30×10^{-3} m^2. The unit of ΔB_{op} as calculated from (3.3) is in tesla, or 10^4 gauss.

3.4.3 Hall Probe Measurement

Another way to determine the flux increment due to DFI operation is to measure the magnetic field density at the center of the magnet directly using a hall probe with its sensing surface perpendicular to the axis of the magnet. Very similar to the integrated values in the two previous measurement methods, the output voltage of the hall probe increases step by step due to the flux injection to the system. The sensitivity of the hall probe, which increases by 0.06 % per degree drop in temperature according to the specification, was calibrated at room temperature (300 K) using a test coil, whose dimensions and magnetic field distribution were known with great accuracy. In this case, for the liquid helium environment, the sensitivity turns out to be 0.218 V/T for a sensing current of 1 mA.

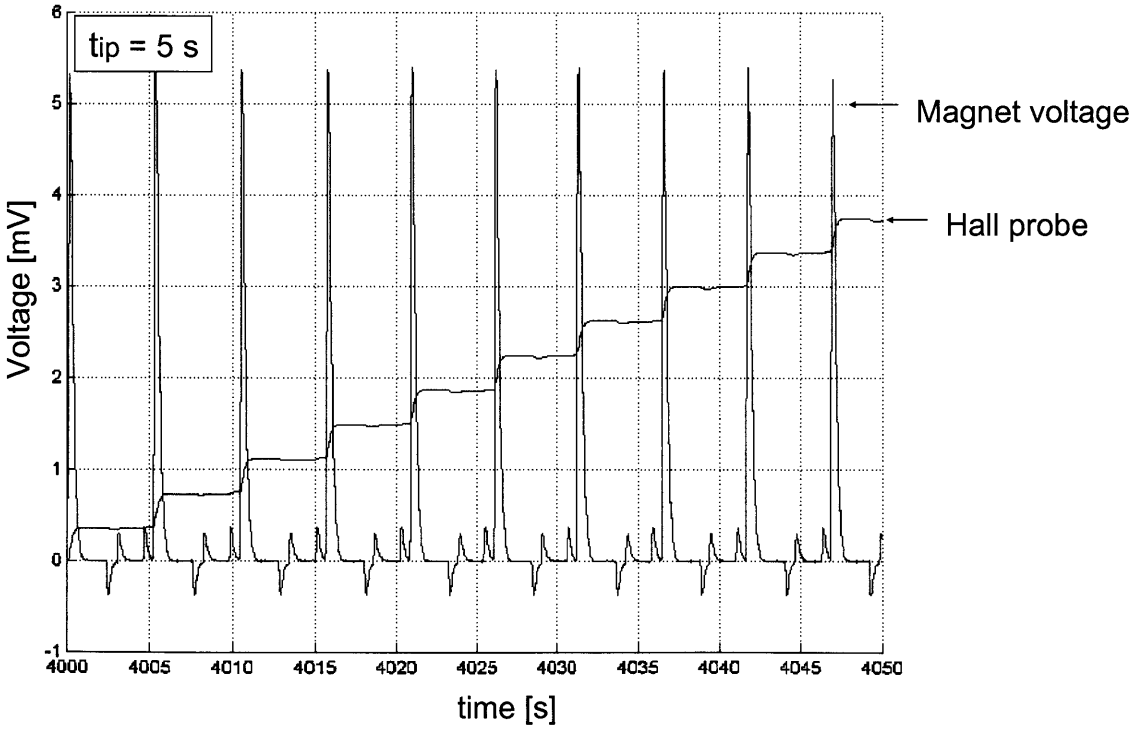

Figure 3-5 Typical plots for the induced insert magnet voltage ("spikes") and the flux increment ("steps") for a series of DFI injection cycles each with a period of 5 seconds. The flux increments is proportional to the time integral of the insert voltage.

Chapter 4

Results and Discussion

4.1 Design Objectives

The full-scale digital flux injector was designed based on the prototype with major parameters modified in order to meet two objectives:

- Ability to compensate dissipations in the Phase 1 HTS insert coil;
- Physical compatibility with the Phase 1 LTS/HTS NMR system.

While dissipations in the HTS insert can come from several areas, the total resistance of the BSCCO-BSCCO splices between the 50 double-pancake modules in the insert was assumed to be the dominant contribution, and its value was measured to be 1.5 μΩ in another experiment performed earlier [6]. Also, since the DFI operation with the NMR insert will eventually be tested in the presence of the Phase 1 NMR background magnet, the design of the DFI must satisfy the physical constraints imposed by the Phase 1 system, i.e. clearance for the room-temperature bore and maximum limit on outer diameter.

In compliance with these requirements, the primary and secondary DP coils of the DFI were designed, wound, and assembled. Superconducting switches connected with the secondary coil were designed and made to regulate the flux injection cycles. The DFI unit was first coupled and operated with an LTS insert magnet, and then with the Phase 1 HTS insert. The performance of the DFI in both cases was measured and evaluated.

4.2 Switch Response

The successful operation of the DFI depends on the critical step of current commutation between the secondary coil and the insert, which is controlled by the superconducting switches opening and closing in the proper sequence. This is accomplished by inputs of appropriate current profiles and by effective cooling with effluent helium vapor.

Fig.4-1 shows the actual current profiles for the primary coil and the heaters for switches S_2 and S_3 for two complete cycles. These profiles were controlled by the digital outputs of LABVIEW with three separate programmable KEPCO power supplies. The primary coil current induces current in the secondary coil and determines the magnitude of flux increment that is possible during current commutation. During DFI operation, I_p was set to about 8.6 A for the LTS insert coil and about 10 A for the HTS insert coil, and the current for the switch heaters was set to 2 A for a duration of 0.5 s.

The temperature and voltage measurements of the switch S_2 during the injection are illustrated in Fig.4-2. Initially, the temperature is at 5 K, near the ambient temperature. The primary coil current is first established to induce current in the secondary coil, and then the heating current for S_2 is turned on. Temperature starts to increase immediately, reaches a maximum of 20 K as heating stops, and then decreases back to the ambient temperature. The switch voltage, essentially the same as the voltage across the insert, comes up as the S_2 temperature exceeds a critical value of 12 K. With S_2 becoming an open circuit, current commutation starts and lasts until the temperature drops below 12 K and S_2 becomes superconducting again. After that, the primary coil current I_p is shut off. One important thing to note here is that shutting off I_p induces I_s in the secondary coil in the opposite direction as the beginning of the injection cycle. At this point, if S_2 has not completely recovered to its superconducting state, the commutation between the secondary coil and the insert will continue, but now will result in a decrease of I_{op} in the insert, thereby negating the effect of the flux injection earlier. Hence, it is critical to allow sufficient time for S_2 to cool down by the helium vapor before the primary coil current can be shut off. This is not necessary for S_3, however.

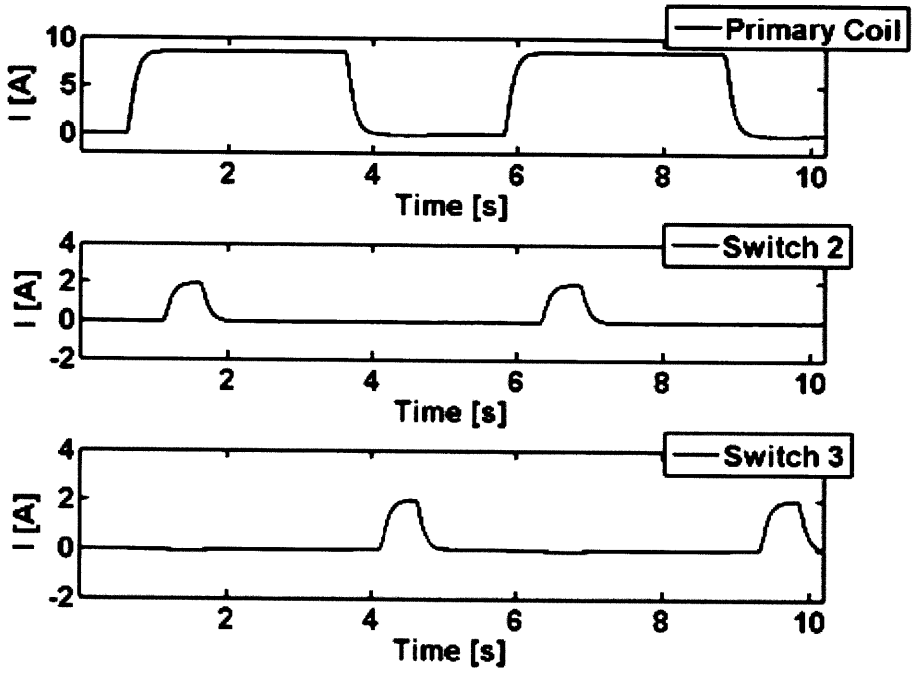

Figure 4-1 Current profiles for primary coil, switches S_2 and S_3 controlled by digital outputs from LABVIEW. The injection period is 5 seconds.

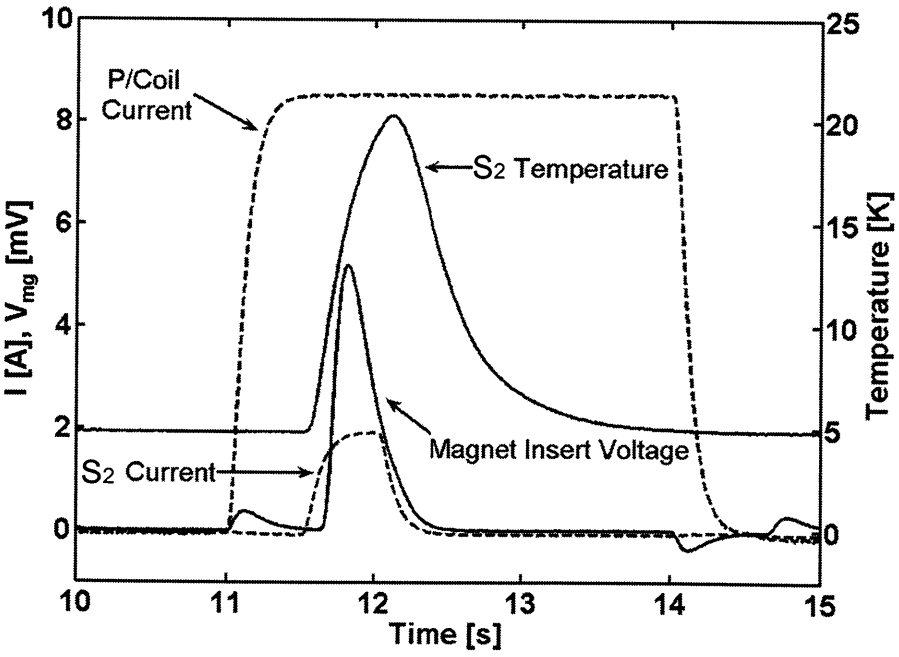

Figure 4-2 Switch S_2 temperature and magnet voltage vs. time during DFI injection.

4.3 Results of Operation with the LTS Insert

For performance calibration purposes, the first full-scale DFI was operated with an LTS insert coil, which has a self inductance of 0.98 H and a magnet constant of 0.021 T/A at the center. During the operation, the liquid helium level was maintained between the LTS insert and the DFI unit at all times to ensure sufficient cooling for the superconducting switches. Therefore, in order to prevent the need for liquid helium refill and possible disturbance to the system, the experiment was started with the liquid helium level just below the two switches S_2 and S_3, and one-and-a-half hour later, stopped when liquid helium was just enough to expose the LTS insert coil. During that period, about 1100 digital flux injections were performed, and as a result, the current in the LTS insert coil increased from zero to 1.87 A, as shown by the hall probe measurement in Fig.4-3. Every single injection or flux pumping shot was detected by the measurement system, but for the purpose of discussion, ten consecutive shots starting at t = 4000 s are presented here for the three independent measurement methods.

Fig.4-4 shows the measurement of the magnetic field at the insert's center by a hall sensor positioned there. From t = 4000 s to t = 4050 s, ten injections each with a period of 5 seconds were performed, and as a result, ten step increments were observed for the hall probe voltage. Using the sensitivity of the hall probe, which was calibrated as 0.218 V/T for a sensing current of 1 mA at liquid helium temperature, the voltage measurement was converted to magnetic flux increments. The average flux increment per shot over the entire course (1100 shots) of the experiment was obtained as 0.036 mT.

Fig.4-5 shows the LTS insert voltage, V_{mg}, from 4000 s to 4050 s, in the upper plot and its numerical integration by MATLAB in the lower plot. Note that all the voltage spikes are pretty much identical, demonstrating the stability of this system. The integrated insert voltage can be used to calculate current increment ΔI_{op} using (3.2), which can then be converted to flux increment ΔB_{op} using the insert's magnet constant. In this case, the conversion can be given as (4.1), where the voltage V_{mg} has the unit of mV. After averaging, the magnetic increment per shot was obtained as 0.036 mT.

$$\Delta B_{op} = 0.0214 \int V_{mg} dt \tag{4.1}$$

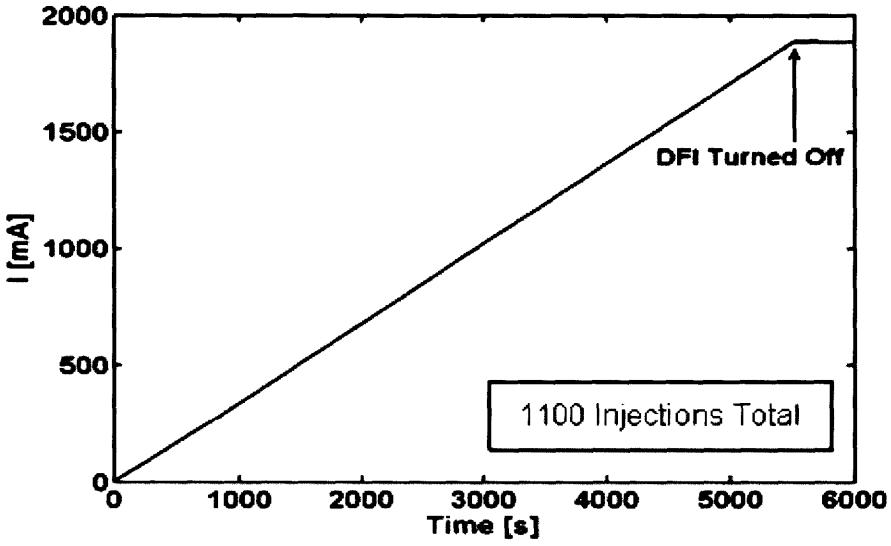

Figure 4-3 LTS insert current vs. time during the experiment.

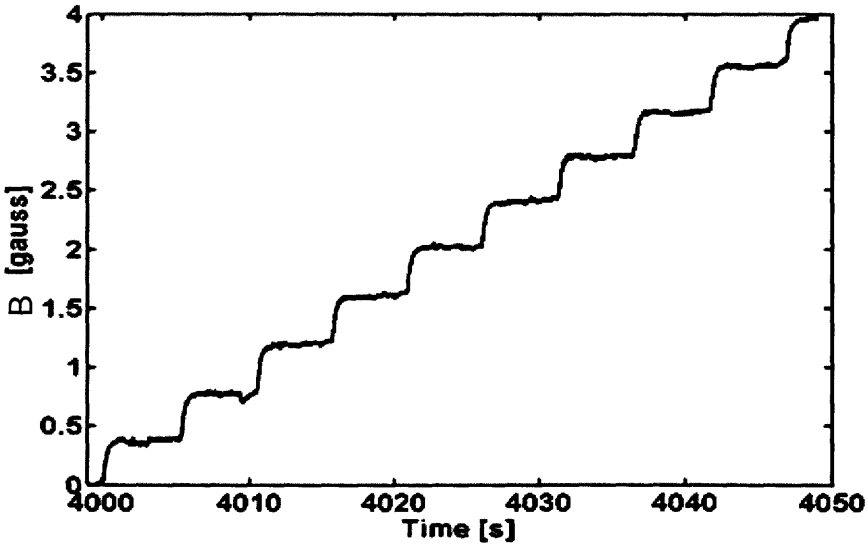

Figure 4-4 Flux density increment measured by hall probe for 10 cycles. The unit is in gauss (1 gauss = 0.1 mT).

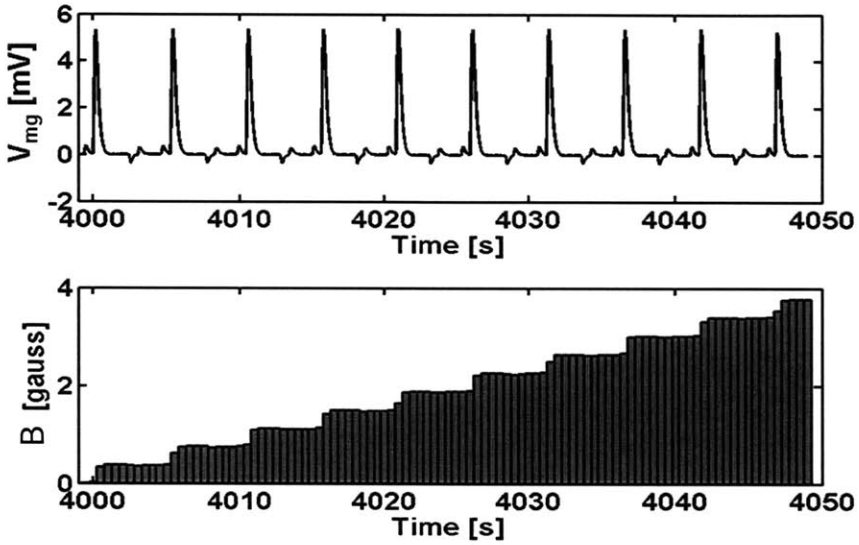

Figure 4-5 LTS insert voltage and flux density increment for 10 cycles. The unit is in gauss (1 gauss = 0.1 mT).

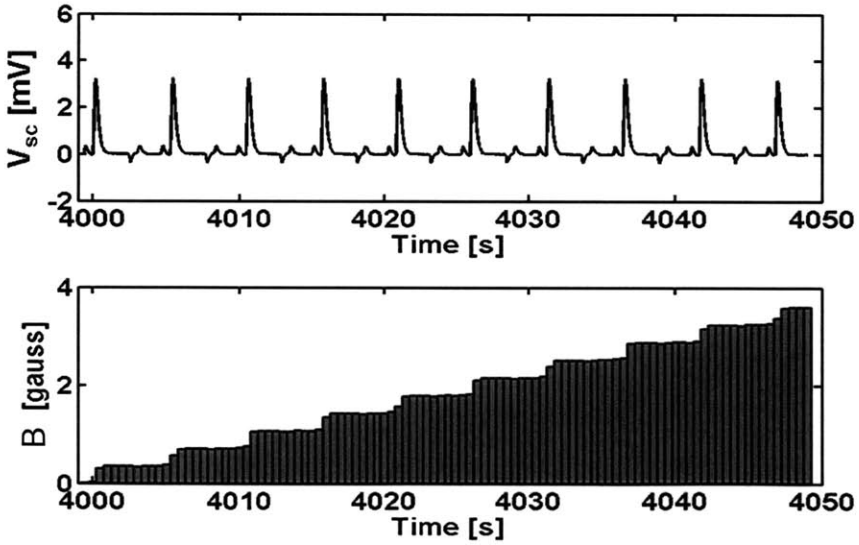

Figure 4-6 Search coil voltage and flux density increment for 10 cycles. The unit is in gauss (1 gauss = 0.1 mT).

Table 4.1 Summary of DFI measurement and calculation results for the LTS case

measurement method	measurement raw value	flux increment per shot [mT]	current increment per shot [mA]	% difference from analysis
Insert Voltage	1.68 [mVs]	0.036	1.71	14
Search Coil	1.05 [mVs]	0.034	1.64	9
Hall Probe	0.078 [mV]	0.036	1.72	15
Analysis	--	0.032	1.50	--

Fig.4-6 shows the search coil voltage measurement, V_{sc}, and its integration. Note that the search coil voltage plot is almost the same as the insert voltage, except for the smaller magnitude of the spikes. Indeed, as calibrations before the test indicate, the two voltages can be converted to each other by a factor of 1.6. The amount of flux injected per shot can also be found from the integrated search coil voltage by (3.3), and after substituting the values for the number of turns and the effective area, (4.2) can be obtained. The estimate for the average flux increment per shot turns out to be 0.034 mT.

$$\Delta B_{op} = 0.0327 \int V_{sc} dt \tag{4.2}$$

As for theory, ΔI_{op} can be calculated as in (1.7). In this case, since I_{op} is initially zero and remains at low (max. at 1.87 A), and L_s is much smaller than L_{mg}, ΔI_{op} can be estimated by (3.1) and can be converted to ΔB_{op} by the magnet sensitivity. After substituting M_{ps}=169 μH and L_{mg} = 0.98 H, the conversion ratios can be obtained (4.3).

$$\Delta I_{op} = \frac{M_{ps} I_p - L_s I_{op}}{L_{mg} + L_s} \tag{1.7}$$

$$\Delta I_{op} = 172 \times 10^{-6} I_p = \frac{\Delta B_{op}}{0.21 \times 10^3} \tag{4.3}$$

Table 4.1 summarizes the major measurement results as well as the theoretical values obtained from (3.1). While the results from the three different methods are within 9-15% of the theoretical ones, they agree remarkable well with each others based on data averaged over 1100 pumping shots.

4.4 Results of Operation with the HTS Insert

After the operation of DFI with the LTS insert coil showed satisfactory performance and excellent agreement with theory, the next step was to operate with the Phase 1 HTS insert coil, which has a self inductance of 1.12 H and a magnet constant of 0.0256 mT/A. The LTS insert was removed and the HTS insert was attached to the DFI system. Joints were made between the Nb_3Sn tape of the DFI and the BSCCO-2223 tape of the HTS insert by overlapping and soldering. One side of the stainless steel reinforcement layers of the BSCCO was removed prior to overlapping, and to avoid contamination, the original solder on the BSCCO tape was used to solder the Nb_3Sn tape. For the Nb_3Sn tape, its copper layer was left intact to protect the brittle Nb_3Sn material from possible damage during the joint-making process. After the joints were made, the same procedure as in the LTS insert experiment was followed to prepare the system ready for DFI operation.

Initially, the HTS insert was uncharged and by DFI operation, magnetic flux was injected into the system. Fig.4-7 shows the operating current increments in the HTS insert during the first ten DFI injection cycles with a period of 5 s. The upper plot shows the step increments of the operating current, I_{op}, in the HTS insert coil, obtained from the magnetic field measurements by a hall probe at the center. The bottom plot shows the profiles of the actual primary coil current, I_p, which had an on-state level of 10.8 A. As expected, the increments look very similar to those in the LTS insert experiment except the magnitudes of the increments affected by the different self inductances and primary coil currents. In this case, for the idle HTS insert, the ΔI_{op} was about 2 mA per cycle, or 0.4 mA/s. ΔI_{op} can also be estimated analytically using equation (1.7). After the substitution with corresponding values in the HTS experiment, an expression which relates ΔI_{op} and I_{op} can be obtained as in (4.4). As I_{op} increases in the insert, ΔI_{op} will decrease. For the uncharged insert, I_{op} is zero, and 1.64 mA is predicted for ΔI_{op}.

$$\Delta I_{op} = (1642 - 15.2 I_{op}) \times 10^{-6} \tag{4.4}$$

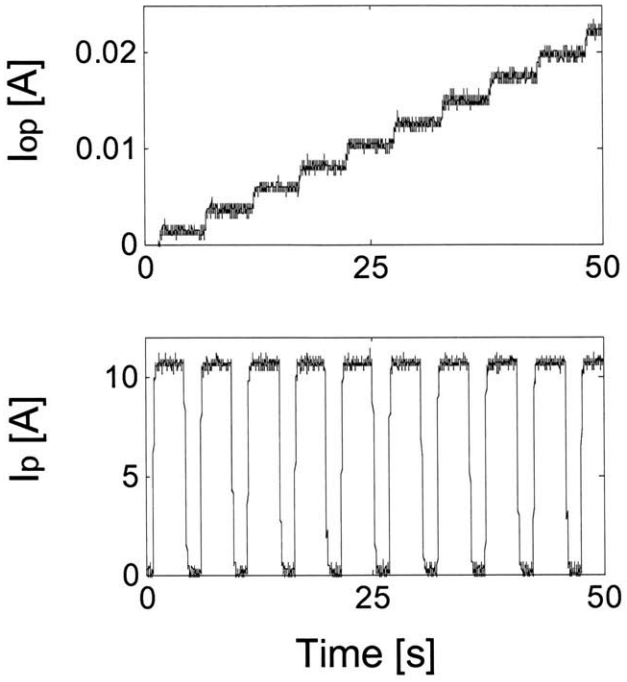

Figure 4-7 HTS insert current vs. time during DFI operation.

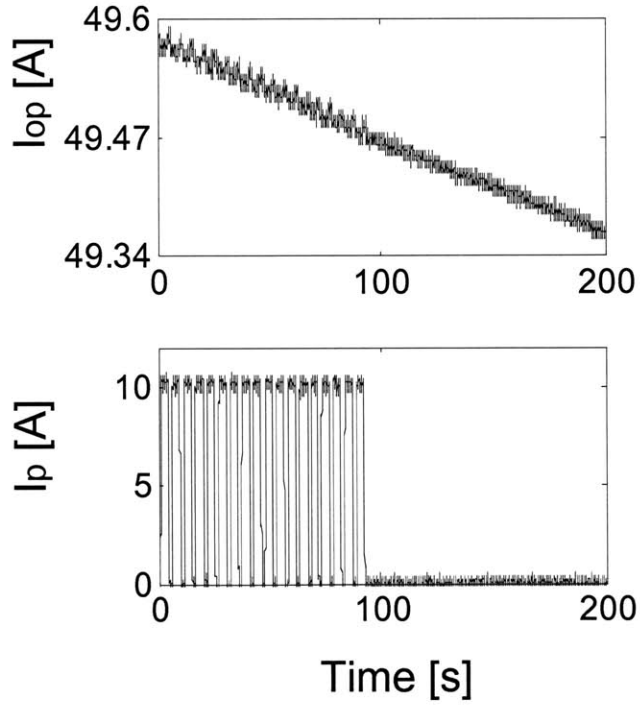

Figure 4-8 HTS insert current vs. time for I_{op} = 50 A, with and without DFI injection.

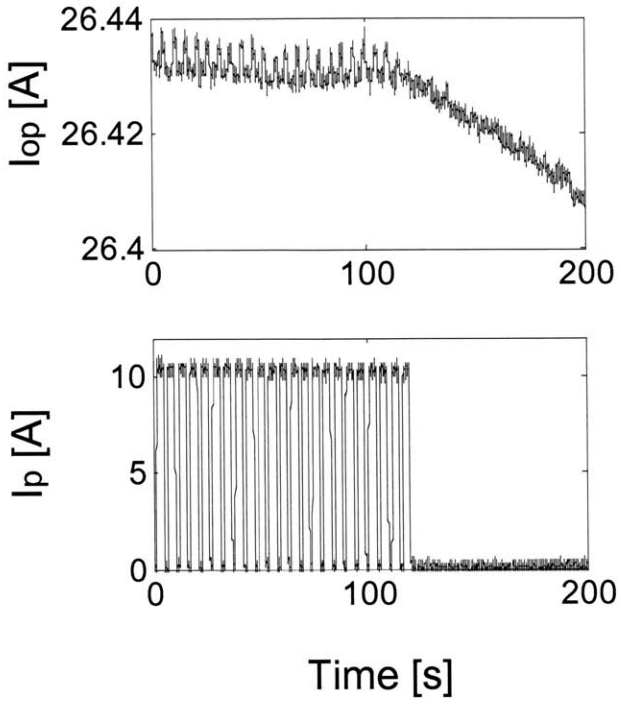

Figure 4-9 HTS insert current vs. time for I_{op} = 26 A, with and without DFI injection.

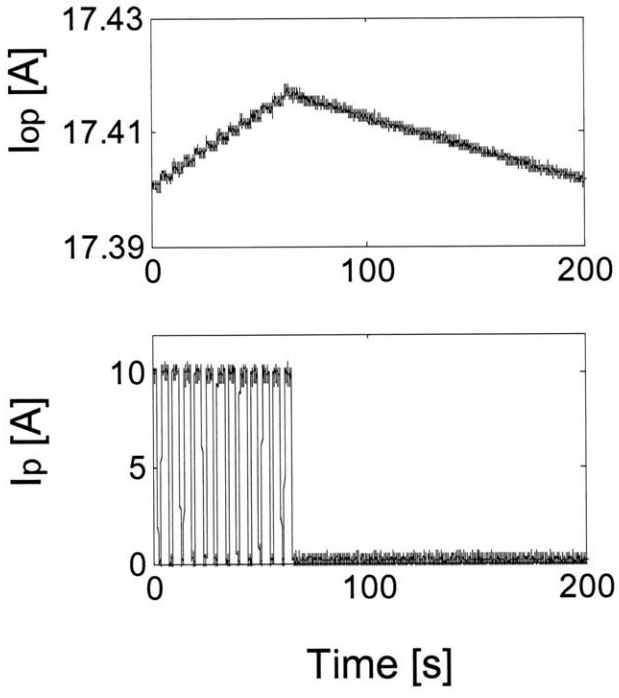

Figure 4-10 HTS insert current vs. time for I_{op} = 17 A, with and without DFI injection.

Table 4.2 Summary of DFI measurement and calculation results for the HTS case

Magnet Current	50 A	26 A	17 A
Injection Rate [mA/s]	0.18	0.25	0.28
Self Decay Rate [mA/s]	1.0	0.26	0.11
Time Constant [s]	50,000	100,000	160,000
Effective Resistance [μΩ]	20	10	6

The HTS insert was charged up to its normal operating current of 50 A by an external power supply, during which the superconducting switches S_2 and S_3 were heated by a current of about 3 A and maintained at temperatures much higher than the critical temperature of the Nb_3Sn tape. After that, the switch heaters were turned off, S_2 and S_3 returned to the superconducting state, the external power supply was removed, and liquid helium was refilled to its initial level just below the switches. Unlike the LTS insert, since the HTS insert has significant dissipations, its magnetic field and operating current would decay naturally as described by (2.1) at a rate of dI_{op}/dt, which is a function of I_{op}. As the hall probe continuously monitored the magnetic field at the center, the self decay rate at 50 A was determined with DFI remaining idle. When DFI operation started, the effect of the flux injections on the insert was observed. I_{op} was reduced first to 26 A, and then to 17 A, by heating up the two switches and creating additional dissipations in the system. At each level, the same procedure was followed to measure the self decay rate and the DFI performance. The measurements are plotted in Figs.4-8, 4-9 and 4-10, and their results are summarized in Table 4.2.

For I_{op} = 50 A, the self decay rate dI_{op}/dt was measured as 1.0 mA/s, whereas the theoretical injection rate $\Delta I_{op}/t_{ip}$, calculated from (4.4) and t_{ip} = 5 s, was only 0.18 mA/sec. Therefore, DFI operation was unable to fully compensate the much faster dissipations in the insert, as shown in Fig.4-8. The time constant of the self decay could be calculated as (4.5), and the effective circuit resistance was obtained as 20 μΩ.

$$\tau = \frac{I_{op}}{\left|dI_{op}/dt\right|} = \frac{L_{mg}}{R_{cir}} \tag{4.5}$$

For I_{op} = 26 A, dI_{op}/dt was measured as 0.26 mA/s, and $\Delta I_{op}/t_{ip}$, which increases with decreasing operating current, turned out be 0.25 mA/s. As a result, the DFI operation was almost enough to fully compensate the self decay as shown in Fig.4-9. As self decay became slower, the time constant was increased, and the effective resistance was calculated as 10 μΩ.

Finally, for I_{op} = 17 A, the decay rate dropped further to 0.11 mA/sec, while the injection rate increased to 0.28 mA/s. As shown in Fig.4-10, DFI operation was able to compensate and actually increase I_{op}. In this case, the effective resistance was 6 μΩ.

4.5 Dissipations in the HTS Insert

While the magnitudes of flux injections by DFI were as predicted in theory, the self dissipations in the HTS insert happened to be much faster than expected. The effective circuit resistance, R_{cir}, which was assumed to be 1.5 μΩ and mostly due to splices in the HTS insert, turned out to be much larger and strongly dependent on the operating current. In order to better understand the source of these dissipations, each contribution to R_{cir} was re-evaluated in experiments separate from the DFI system . There are three main contributions of resistance in the DFI-HTS system, as given in (4.6).

$$R_{cir} = R_j + R_{sp} + R_n \tag{4.6}$$

Where, R_j is the resistance of the joints between the Nb_3Sn tape and the BSCCO tape;

R_{sp} is the resistance of the 49 splices between double pancakes in the insert;

R_n is the effective resistance due to the index dissipation in the insert.

Firstly, R_j was evaluated in a "trapped field" test for similar Nb_3Sn-BSCCO joints in a DP test coil. Secondly, the V-I characteristic for each splice in the insert was obtained to calculate R_{sp}. Thirdly, the V-I characteristic for each DP in the insert was measured to calculate the I_c and n values, which can be used to find out R_n by (1.4).

4.5.1 Joint Resistance Test

The experiment setup of the joint resistance test is shown in Fig.4-11. It consists of a thin double pancake coil with six turns inside a cryostat, a charging magnet outside the cryostat, and a hall sensor at the center to measure the magnetic field. The DP coil was wound with the same type of BSCCO tape as the Phase 1 HTS insert and its two open ends on the outside were joint together by a piece of Nb_3Sn tape to form a closed loop. A heater was wrapped around the joint section to increase the temperature of the coil as necessary. The procedure of the trapped-field test can be described as the following:

- The DP coil is positioned at the center of a charging magnet;
- Magnetic field is established by the charging magnet;
- After liquid helium transfer, the DP coil becomes superconducting;
- The charging magnet is shut off and magnetic field is trapped;
- The self decay rate of the trapped field is measured;
- The time constant and resistance of the joint are determined.
- The Heater is turned on, and the trapped field is discharged.

Fig.4-12 shows the magnetic field measurement and the charging current profile during the trapped-field test. A magnetic field of 18 mT was first established by the charging magnet, and 10 mT was trapped by the DP coil after the charging magnet was shut off. The decay rate of the trapped field was obtained as 0.625 μT/s, equivalent to a time constant of 16,752 s. From the time constant and the inductance of the DP coil, which is measured as 30.14 μH, the resistance of the joint was calculated as 1.8 nΩ.

While the joints tested here were made the same way as the joints between the DFI and the HTS insert, the current and the magnetic field conditions for the joints were different. During the DFI operation, a larger current was flowing through the joints, but if Ohm's law was assumed to be applicable in this case for the joint resistance, then there would be no effect due to the current. Also, since the locations of the joints were high above the insert coil and exposed to a much reduced field, the effect of field on joint resistance could be neglected. Hence, R_j, which could be estimated to be on the order of nano-ohm, would have negligible contribution to the overall circuit resistance.

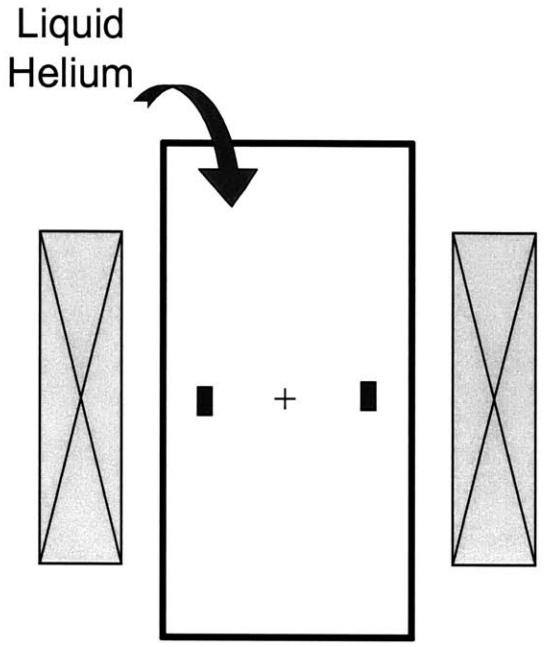

Figure 4-11 Schematics of the trapped field test for measuring the joint resistance.

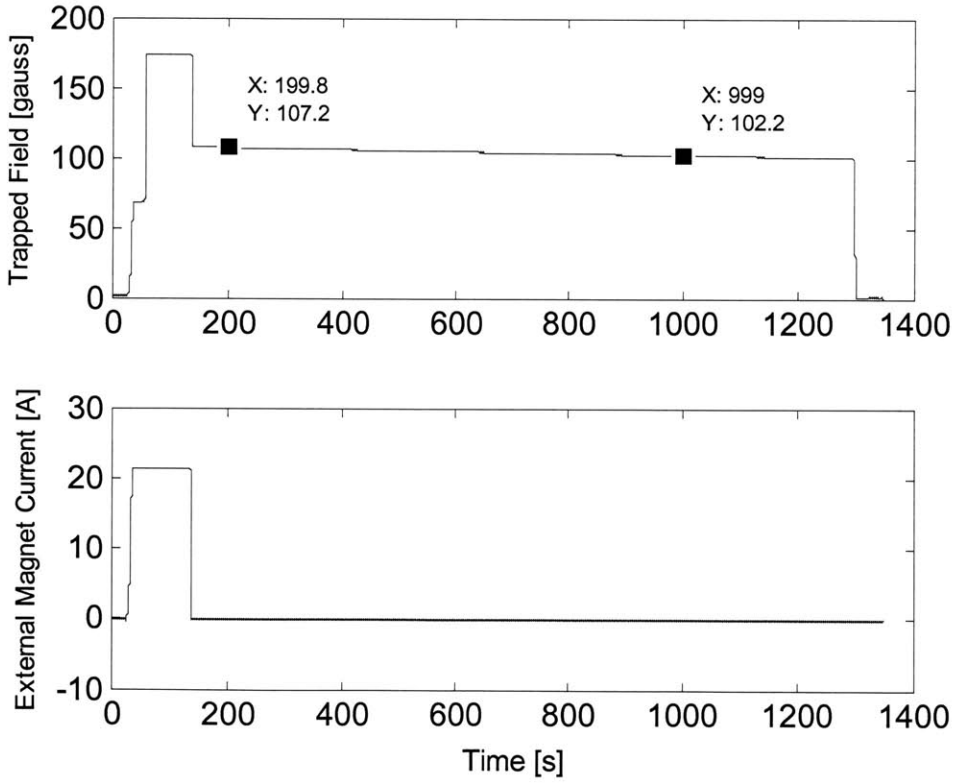

Figure 4-12 Magnitude of trapped field vs. time (top plot); external magnet current profile vs. time (bottom plot).

4.5.2 Splice Resistance Test

Fig.4-13 shows the schematics of the HTS insert consisting of double pancake modules spliced together. Voltage taps were put on both ends of all the splices and could be used to measure the V-I characteristics of all splices. Note that the same voltage taps, when paired up differently, could be used to measure the voltage across all double pancakes, and this was done for the index resistance measurements in the next section.

The majority of R_{sp} comes from a few bad splices. The objective of the splice resistance test, therefore, was to obtain the V-I curve for each splice and to identify the bad ones. Measurements were first done in liquid nitrogen and later in liquid helium. During the test, the current in the HTS insert was increased from zero to a significant level at a constant rate using a magnet power supply. Due to the number of data acquisition channels available, seven splices were tested at one time. The results of one of the test runs in liquid nitrogen are shown in Fig.4-14 and tabulated in Table 4.3. In this particular case, the voltage of one splice increased very sharply with current, indicating a bad splice. The resistance of the splice was estimated by the slope and turned out to be 2.175 μΩ. For the liquid nitrogen case, the resistance for all 49 splices added up to 21.3 μΩ, with 8 bad splices contributing about 90% of the total resistance.

The measurement was repeated in liquid helium, and the same bad splices were identified. However, the resistance values were lower this case because of the lower temperature, and the total splice resistance turned out to be 4.4 μΩ. Since the V-I curves were pretty much linear in all cases, it could be reasonably assumed that R_{sp} is independent of the operating current. Comparing with the previous measurement value of 1.5 μΩ, it is apparent that some level of degradation had occurred due to mishandling during assembly, disassembly and movement since that measurement.

The new value of R_{sp} = 4.4 μΩ also agrees reasonably well with the DFI operation results discussed in the previous section. At I_{op} = 17 A, the index dissipation should be minimal due to the low current ratio, and also the joint resistance was insignificant as already discussed, therefore, the splice resistance should account for most of the effective circuit resistance (R_{cir} = 6 μΩ) and it did.

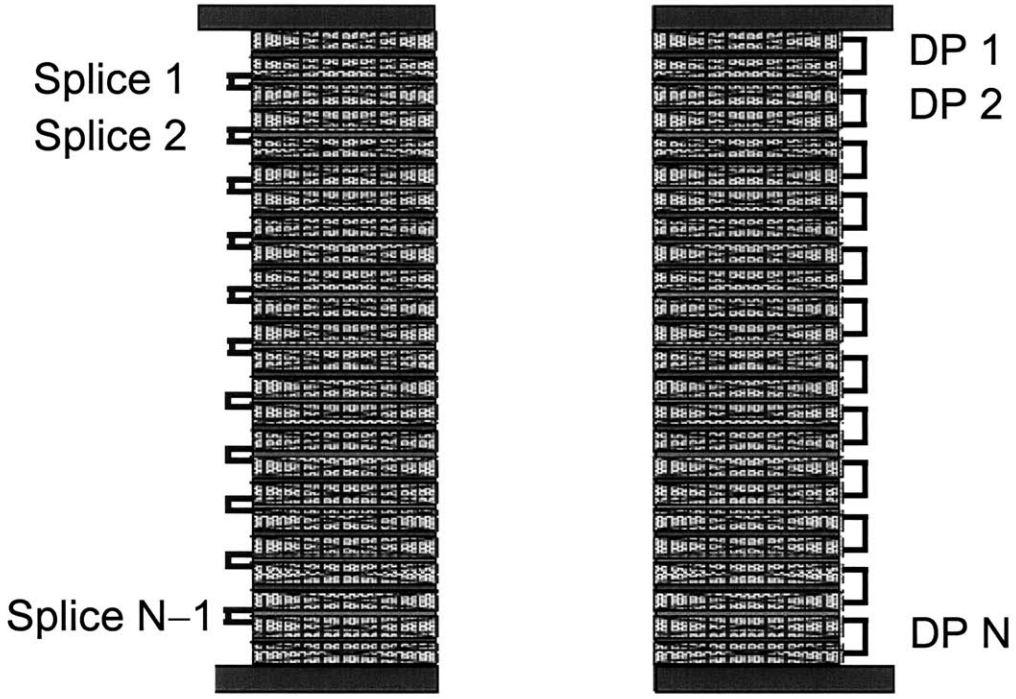

Figure 4-13 Schematics of DP modules and splice connections for the HTS insert [3].

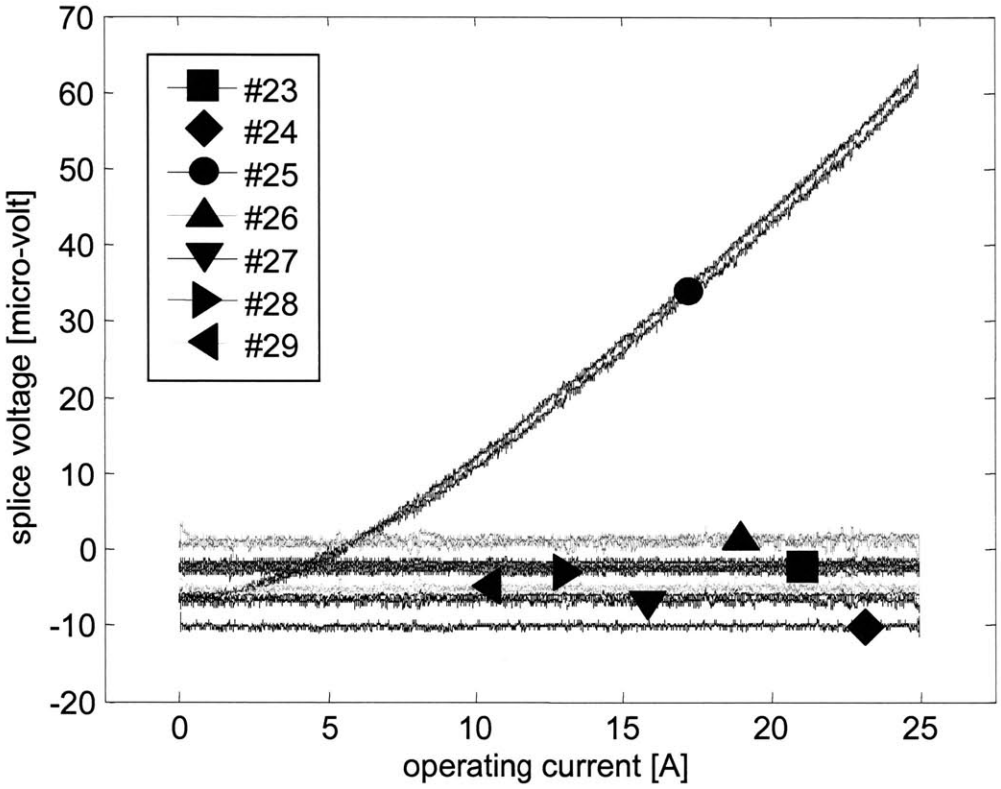

Figure 4-14 V-I characteristics for splices #23 to #29 in the HTS insert.

Table 4.3 Resistance values for splices #23 to #29 at 77 K

Splice between DP #			R [μΩ]
23	--	24	0.011
24	--	25	0.003
25	--	26	2.175
26	--	27	0.018
27	--	28	0.015
28	--	29	0.010
29	--	30	0.015

4.5.3 Index Resistance Test

From the performance results of the DFI and the above-mentioned estimates for the joint resistance and splice resistance, the magnitude of the index resistance could be estimated even before any index resistance test. Since R_j is on the order of nano-ohm and R_{sp} = 4.4 μΩ is invariant with the operating current, this implies that the increase of R_{cir} with higher current levels should be mostly due to R_n, which as given in (1.4) does increase with increasing operating current. As a result, R_n could be roughly estimated as 15 μΩ at I_{op} = 50 A, and 5 μΩ at I_{op} = 26 A.

$$R_n = \frac{V_c}{I_c} n \left(\frac{I_{op}}{I_c} \right)^{n-1} \tag{1.4}$$

If the values of R_n were to be obtained through actual measurements, then according to (1.4), the values for the critical current I_c and index number n would first need to be determined. Since I_c and n values are generally affected by the magnetic field to which the material is subjected, for the HTS insert, each DP coil and theoretically each point will have a different value for I_c and n. Hence, the total effective resistance due to index dissipation can be evaluated accurately only as an integral over the entire volume of the magnet. A lesser accurate estimate of the overall index resistance would be adding up the individual resistance values for each DP in the insert, which could be obtained by (1.4) once the I_c and n values for each DP are known.

Fig.4-15 shows the V-I measurement for the top DP coil in liquid nitrogen, from which I_c and n were calculated. The individual points on the V-I curve were obtained by setting the operating current constant and measuring the voltage; since the inductive voltage was zero for constant current and there was no resistance for the superconducting DP coil, only the voltage due to index dissipation was recorded. During test, the current levels were incremented step by step until the voltage became significantly higher than the critical voltage V_c. Then the measurement points were curve-fit by a power function to determine the values of I_c and n, and for this particular DP coil in liquid nitrogen,

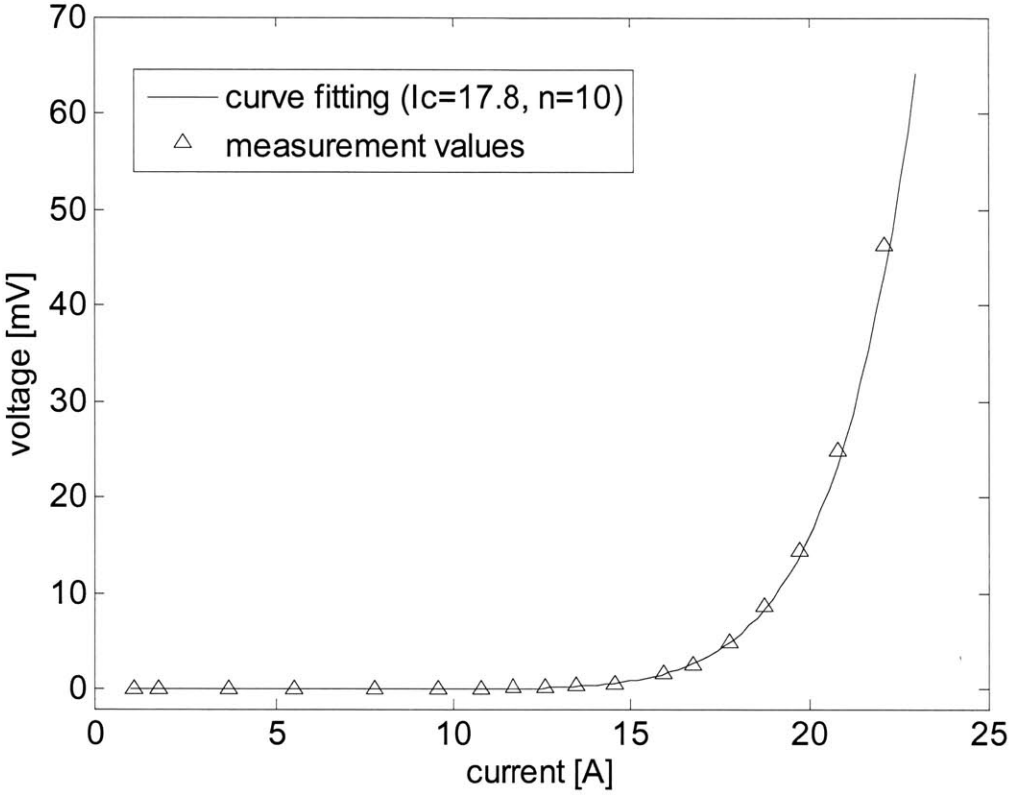

Figure 4-15 V-I measurement values for the top DP coil and curve-fitting results.

they turned out to be I_c = 17.8 A and n = 10. Since the top and bottom DP coils are usually affected the most by the self field of the magnet, I_c = 17.8 A would be the minimum critical current and the limiting factor during normal operation of the insert. In order to estimate the overall index resistance, the I_c and n values of the other DPs would still need to be determined. However, in the process of finding out the I_c values for the DPs located towards the center of the insert, the operating current would necessarily have to be significantly higher than the I_c values for the top and bottom DPs; this would essentially quench DPs and run the risk of overheating and damaging the material. Out of this consideration, the I_c and n measurements for the other DPs were abandoned. The situation would be the same for the liquid helium measurements, except in this case, the I_c values would be considerably higher.

Even if the values for I_c and n were obtained for all the DP coils in the insert, they would be different when the insert is operated with the background NMR magnet because the magnetic field distributions would be different. Therefore, unless the exact values of I_c and n are known for that system configuration, it would probably be more convenient to be able to adjust the flux injection capability of the DFI (by changing primary coil current and switch frequency) for different levels of dissipation. Meanwhile, the Phase 1 HTS insert, as well as any future HTS insert, should be handled carefully and properly to prevent possible degradation.

4.6 Further Considerations

4.6.1 Temporal Stability of the NMR Magnet

The DFI was initially designed to compensate a slightly resistive insert coil in an NMR magnet system so that the insert could be effectively operated in a persistent mode. However there is one more consideration for the performance of the NMR system, which is the temporal stability requirement. Basically, not only do the dissipations in the system have to be compensated, but it has to be done in such a manner that the overall NMR frequency stays within a particular frequency band, $(\left|\overline{\Delta f}\right|/f_o)_{sys}$, for a period of time. Table 4.4 lists the requirements on the DFI injection period (t_{ip}) and the effective circuit

resistance (R_{cir}) for three different frequency bands. For instance, the accepted level of temporal stability for today's NMR magnets is 0.01 ppm/h. In order to achieve this, with the DFI operating at its fullest extent of t_{ip} = 5 s, the system must have a resistance less than 30 nΩ. With DFI operation, however, the resistance would have to be no more than 0.042 nΩ. In the case of the Phase 1 HTS insert, since R_{cir} is in the range of 6-20 μΩ, it is impossible to achieve the temporal stability of 0.01 ppm/h even with DFI injection.

In an ideal case where the splice resistance of the insert can be neglected and the index resistance becomes the only contribution, the operating current ratio I_{op}/I_c and the n value of the insert may be designed to meet the R_{cir} requirement for a given temporal stability as shown in Table 4.5. For example, if R_{cir} = 15 nΩ is required and I_{op}/I_c ratio is at 0.3, then the n value of the insert would have to be better than 10.5.

4.6.2 DFI Operation with the Complete NMR System

While the performance results of the DFI coupled to either LTS or HTS insert coil agree reasonably well with theory, DFI has not been operated with the complete NMR system. Therefore, the effects the NMR background magnet might have on flux injections are yet to be determined. If the background magnet is to be connected in series with the insert, then the flux increments will be much smaller due to the increase in L_{mg}. Also it can be conjectured that since the presence of the background magnet changes the magnetic field distributions in the HTS insert, the I_c and n values for the DPs will change, and as a result, the index dissipations could be different than in the case with only the HTS insert. On the other hand, the DFI injections might have an adverse effect on the temporal stability of the NMR system due to the sharp rate of change in magnetic field during the current commutation. Again, this is yet to be investigated.

The operation of DFI with the complete Phase 1 LTS/HTS NMR system would have been performed if not for the unexpectedly large dissipations in the HTS insert for which the DFI could not compensate. For future investigations, however, DFI can be operated with an all-LTS NMR system using an LTS insert instead. Artificial resistance can be introduced to the LTS insert, for example, by external connections to a shunt resistor.

Table 4.4 Required t_{ip} and R_{cir} values for various $(|\overline{\Delta f}|/f_o)_{sys}$ [5]

$(\lvert\overline{\Delta f}\rvert/f_o)_{sys}$ [ppm]	1	0.1	0.01
t_{ip} [s]	R_{cir} [nΩ]		
5	3000	300	30
10	1500	150	15
15	1000	100	10
30	500	50	5
61	250	25	2.5
151	100	10	1
303	50	5	0.5
3600 *	4.2	0.42	0.042

* DFI not required

Table 4.5 Required n value for combinations of I_{op}/I_c and R_n [11]

I_{op}/I_c	0.9	0.8	0.7	0.6	0.5	0.4	0.3	0.2
R_n [nΩ]	Required n value							
15	120	56.5	35.3	24.7	18.2	13.7	10.5	7.8
10	123	58.3	36.5	25.5	18.8	14.2	10.8	8.1
5	130	61.4	38.4	26.8	19.8	14.9	11.4	8.5
2.5	137	64.5	40.3	28.2	20.8	15.7	12.0	8.9
1	143	67.6	42.3	29.5	21.8	16.5	12.5	9.5
0.5	150	70.7	44.2	30.9	22.8	17.2	13.1	9.9
0.042	173	81.8	51.2	35.7	26.3	19.9	15.2	11.3

Chapter 5

Conclusions

The first full-scale digital flux injector (DFI) has been designed, built and operated with superconducting insert coils for NMR magnets. The operation of DFI with an LTS insert coil has demonstrated that each injection can increment the magnetic field and the operating current of the insert magnet by a quantifiable amount. Results from three independent measurement methods show excellent agreements with the analysis. The operation of DFI with the Phase 1 HTS insert coil has demonstrated that the DFI can compensate dissipations in the HTS insert up to a certain operating current level that is governed by the effective circuit resistance of the insert. Three resistance contributions, from DFI-HTS insert joints, double pancake splices and index dissipations, have been investigated in separate experiments, which has led to a better understanding of their respective magnitudes. Due to unexpectedly poor quality of the HTS insert, the DFI has not been operated with the complete Phase 1 LTS/HTS NMR system. However, for future investigations of the DFI performance in the presence of an NMR background magnet, the DFI can be operated with an all-LTS NMR system using an artificially-made-resistive LTS insert instead.

References

[1] J. Hoffman. Introduction to Superconductors. Online. Internet. January 2006. <http://hoffman.physics.harvard.edu/research/SCintro.php>.

[2] Y. Iwasa. *Case Studies in Superconducting Magnets*. Plenum Press, New York and London, 1994.

[3] Y. Iwasa and J. Minervini. Class lecture and presentation. Massachusetts Institute of Technology, 2005.

[4] J. P. Hornak. *The Basics of NMR*. Online. Internet. January 2006. <http://www.cis.rit.edu/htbooks/nmr/inside.htm>.

[5] Y. Iwasa. Digital flux injectors for superconducting NMR magnets. (Grant application to the NIH National Center for Research Resources, March 1, 2003.)

[6] H. Lee, J. Bascuñán and Y. Iwasa. A high-temperature superconducting double-pancake insert for an NMR magnet. *IEEE Transactions on Applied Superconductivity*, 13: 1546–1549, 2003.

[7] J. Bascuñán, H. Lee, E. Bobrov, and Y. Iwasa. A low- and high-temperature superconducting NMR magnet: Design and performance results. Presented at American Superconductivity Conference, 2002.

[8] Y. Iwasa. Microampere flux pumps for superconducting NMR magnets, Part 1: basic concept and microtesla flux measurement. *Cryogenics*, 41:385–391, 2001.

[9] S. Jeong, H. Lee, and Y. Iwasa. Superconducting flux pump for high-temperature superconducting insert coils of NMR magnets. *Adv. Cryogenic Engr.*, 47:441–448, 2002.

[10] H. Lee, H. M. Kim, and Y. Iwasa. A flux pump for NMR magnets. *IEEE Transactions on Applied Superconductivity*, 13:1640–1643, 2003.

[11] Y. Iwasa (unpublished report, 1998).

Appendix A

SOLDESIGN Calculations

SOLDESIGN V3.0 12/16/ 3 19:14

```
ECHO LIST OF INPUT DATA
  1 setup
  2 ! solenoid, a1, -b, 1, (a2-a1), 2b, NI/[(2b)(a2-a1)], N, 10
  3 ! primary coil
  4 solenoid, 0.03283, -0.0036, 1, 0.01956, 0.0072, 10000, 110, 10
  5 ! secondary coil
  6 solenoid, 0.03098, -0.0036, 1, 0.00107, 0.0072, 10000, 6, 10
  7 end
  8 terminal

 No. Coils =  2 in  2 groups
Time in setup  =  0.000E+00 seconds,      0 loop calculations used
Time in termin =  0.000E+00 seconds,      0 loop calculations used
   1   1     1.3475247D-03      100
   1   2     4.2266715D-05      100
   2   2     4.1663732D-06      100


 TOTAL SYSTEM INDUCTANCE IS =  1.4362245D-03 Henries


Time in induct =  1.000E-02 seconds,      0 loop calculations used
Time in stop   =  1.000E-02 seconds
```

Appendix B

SOLIDWORKS Drawings

8 each

Copper 0.040"

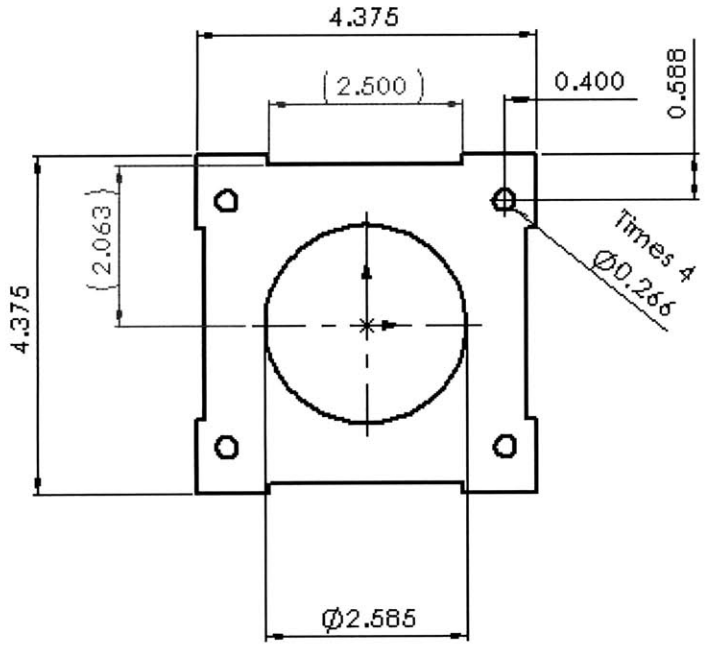

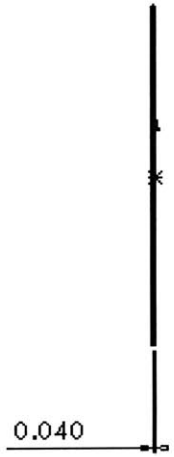

				NAME	DATE	
		DIMENSIONS ARE IN INCHES TOLERANCES: FRACTIONAL ± ANGULAR: MACH ± BEND ± TWO PLACE DECIMAL ± THREE PLACE DECIMAL ±	DRAWN			Copper Insulation -- outside
			CHECKED			
			ENG APPR.			
			MFG APPR.			
		MATERIAL --	Q.A.			
			COMMENTS:			

PROPRIETARY AND CONFIDENTIAL
THE INFORMATION CONTAINED IN THIS DRAWING IS THE SOLE PROPERTY OF

4 each

Copper 0.040"

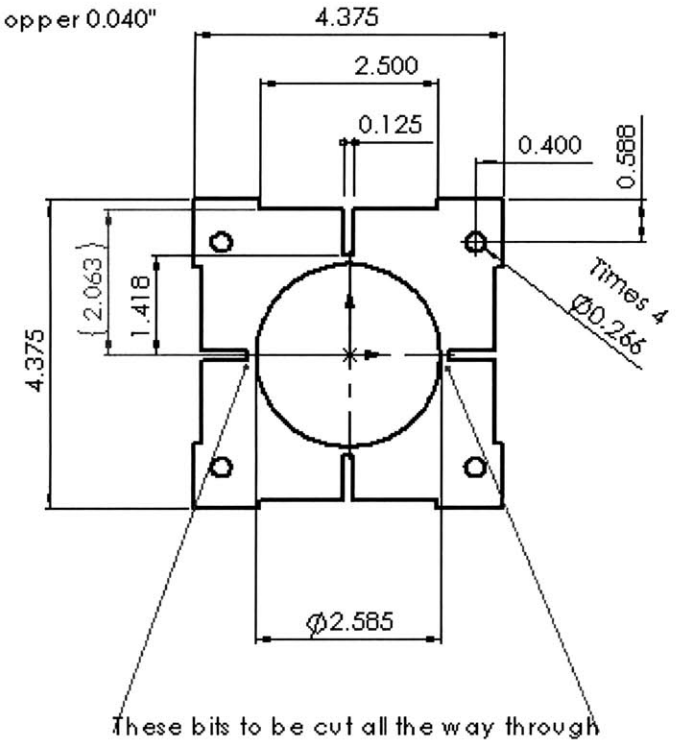

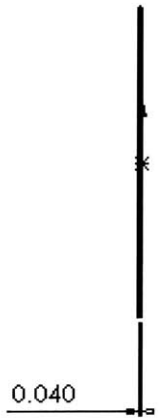

Copper Insulation
-- center

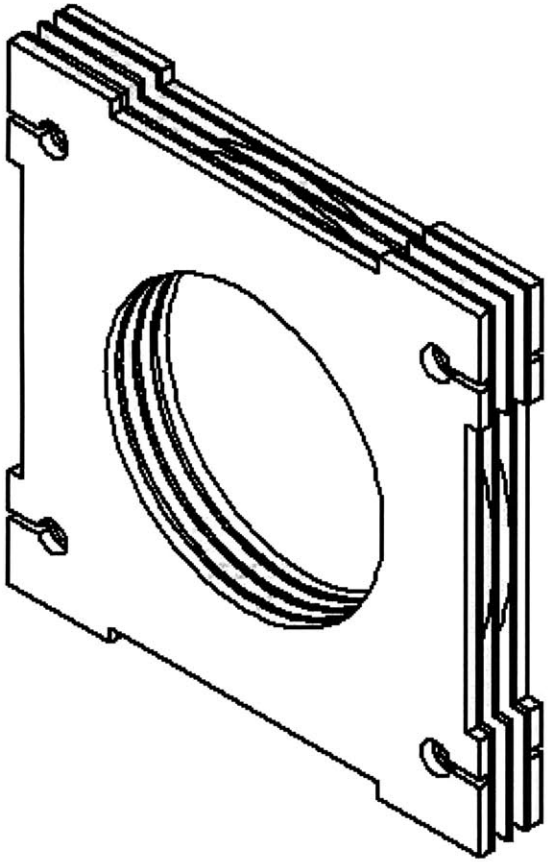

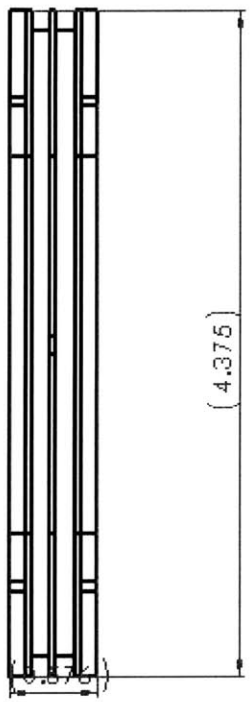

DP assembly (x4)

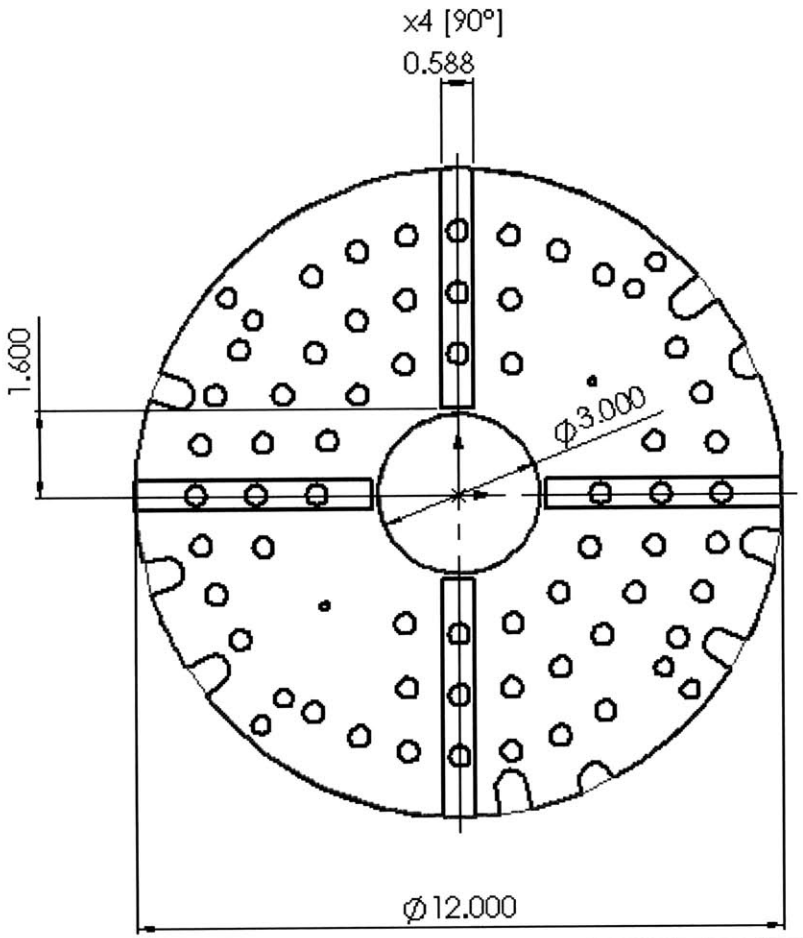

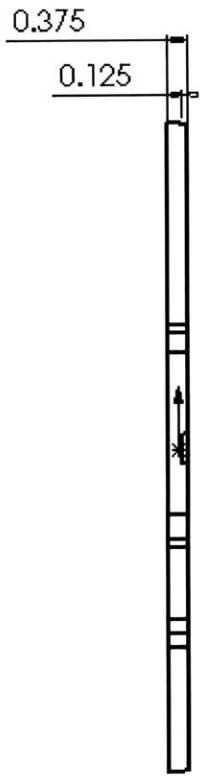

DIMENSIONS ARE IN INCHES
TOLERANCES:
FRACTIONAL ±
ANGULAR: MACH ± BEND ±
TWO PLACE DECIMAL ±
THREE PLACE DECIMAL ±

NAME DATE
DRAWN
CHECKED
ENG APPR
MFG APPR

PROPRIETARY AND CONFIDENTIAL

Top/Bottom Plate
Major Dimensions

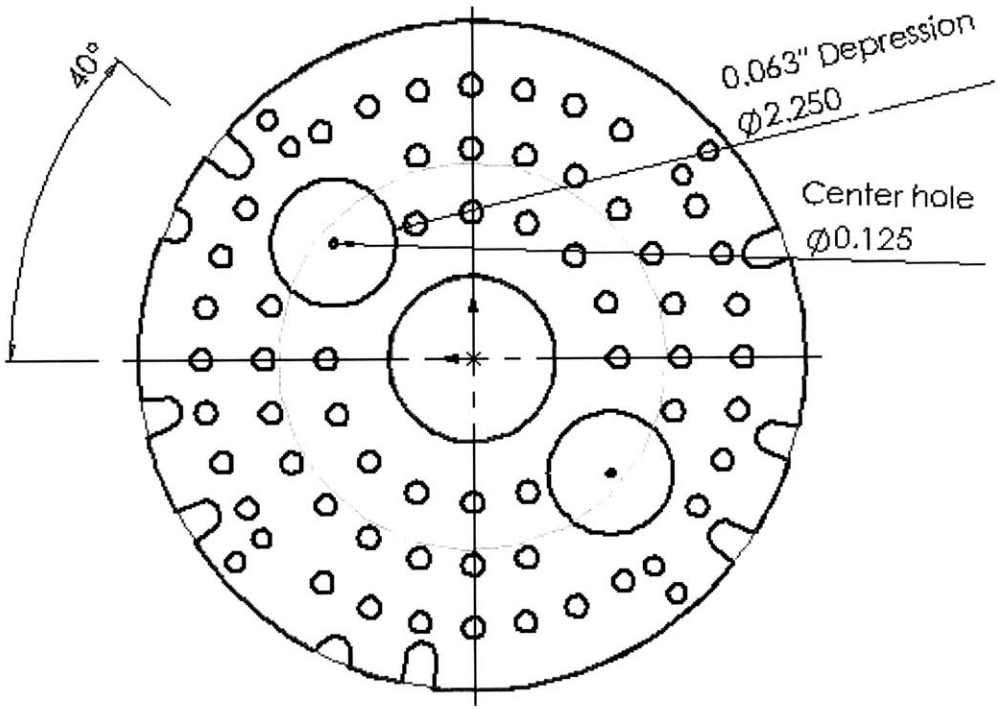

		DIMENSIONS ARE IN INCHES		NAME	DATE
		TOLERANCES:	DRAWN		
		FRACTIONAL ±	CHECKED		
		ANGULAR: MACH ± BEND ±	ENG APPR		
		TWO PLACE DECIMAL ±	MFG APPR		
		THREE PLACE DECIMAL ±	Q.A		
		MATERIAL --	COMMENTS:		

PROPRIETARY AND CONFIDENTIAL
THE INFORMATION CONTAINED IN THIS DRAWING IS THE SOLE PROPERTY OF <INSERT COMPANY NAME HERE>. ANY

Back view of bottom plate (switch location)

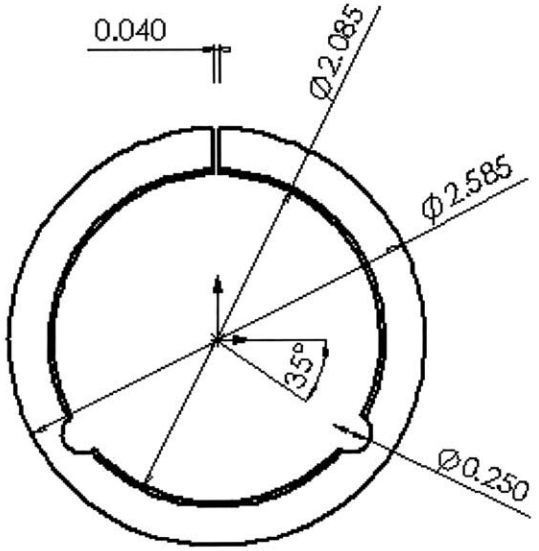

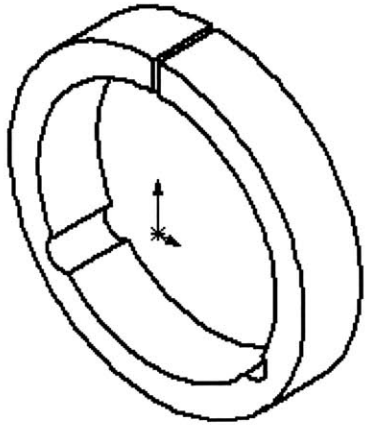

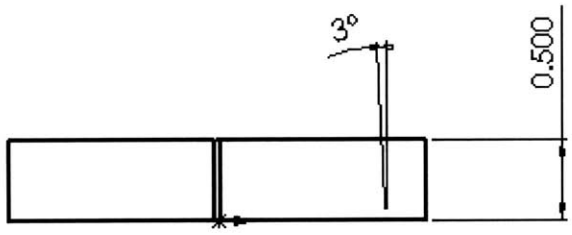

DP Primary Coil Winding Stage
Outer Piece
Filename: stage1.dwg

Quantity: 1
Material: Aluminum

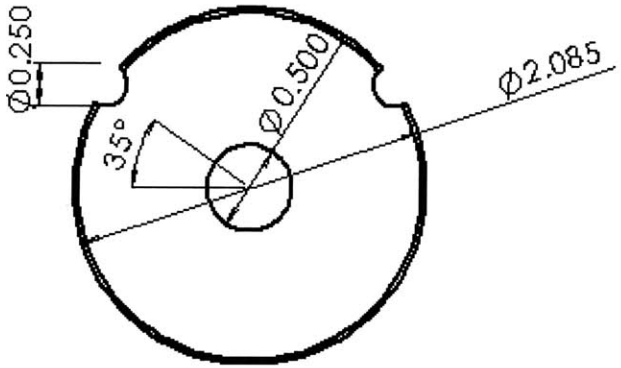

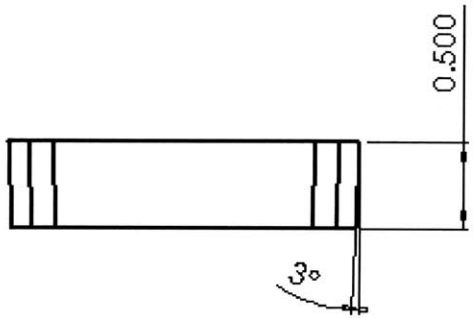

DP Primary Coil Winding Stage
Inner Piece
Filename: stage2.dwg

Quantity: 1
Material : Aluminum

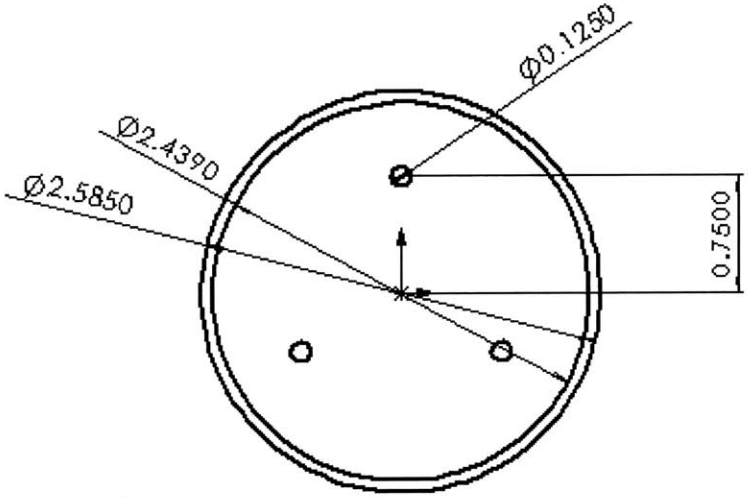

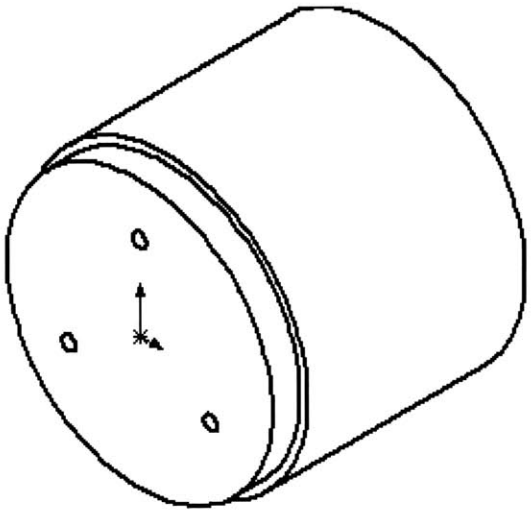

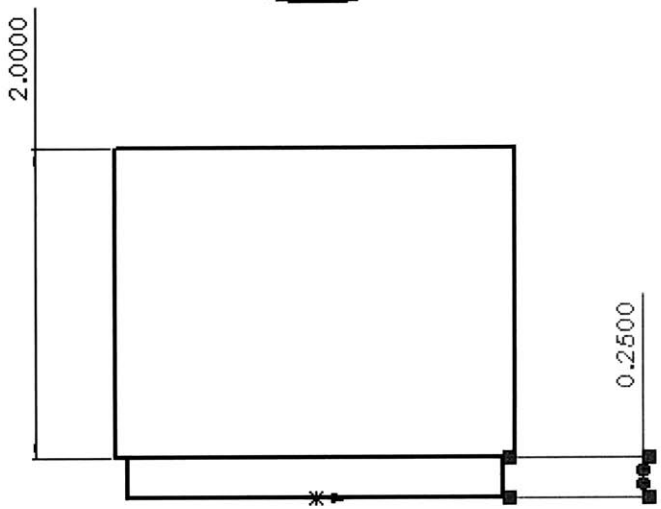

DP Secondary Coil Winding Core
Filename: Winding.dwg

Quantity: 2
Material: flannel wood (we already have)

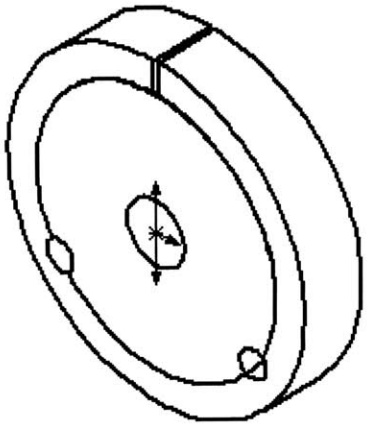

DP Primary Coil
Winding Stage Assembly

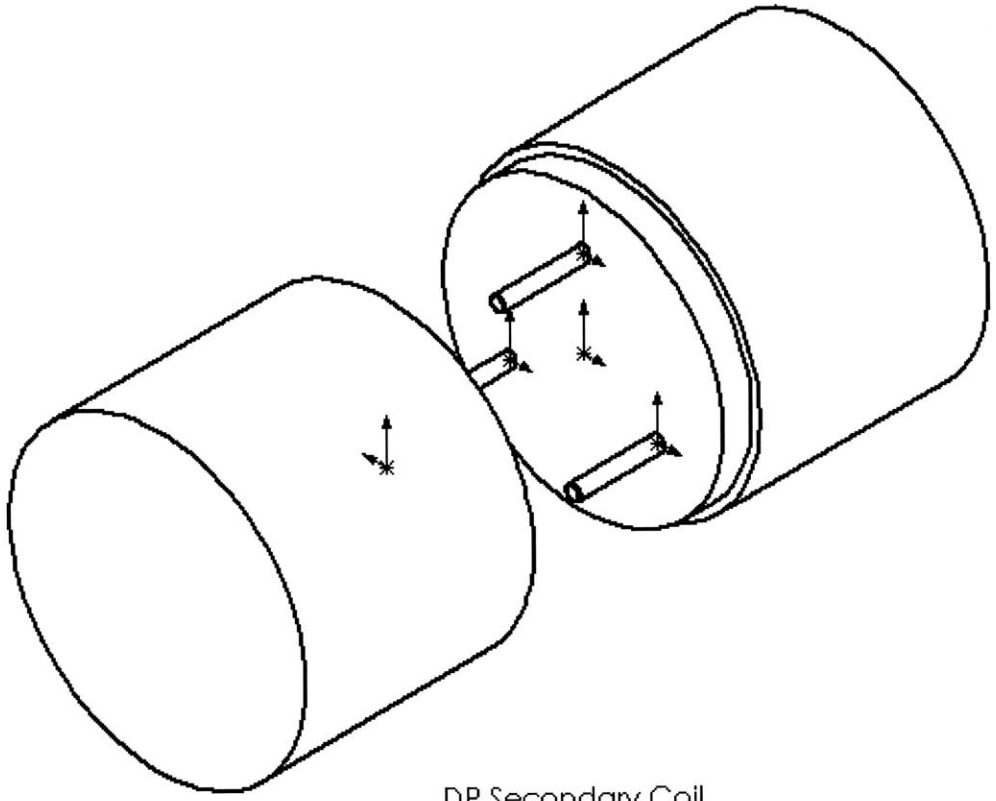

DP Secondary Coil
Winding Core Assembly

2 each

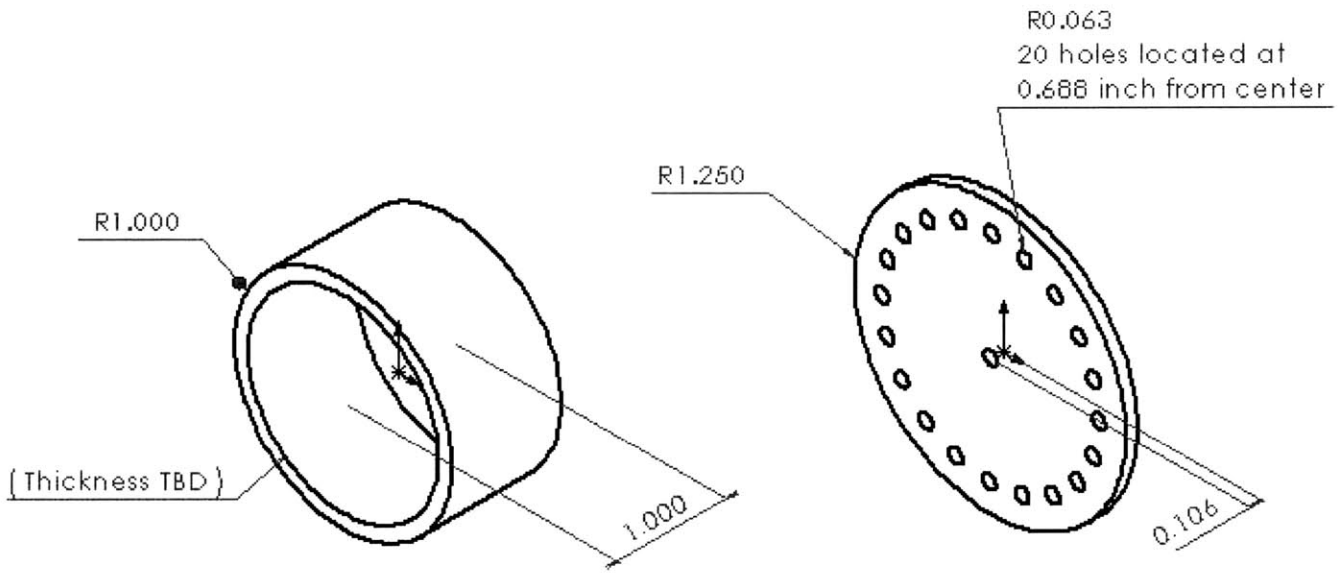

		DIMENSIONS ARE IN INCHES TOLERANCES: FRACTIONAL ± ANGULAR: MACH ± BEND ± TWO PLACE DECIMAL ± THREE PLACE DECIMAL ±		NAME	DATE
			DRAWN		
			CHECKED		
			ENG APPR.		
			MFG APPR.		
PROPRIETARY AND CONFIDENTIAL THE INFORMATION CONTAINED IN THIS DRAWING IS THE SOLE PROPERTY OF <INSERT COMPANY NAME HERE>. ANY REPRODUCTION IN PART OR AS A WHOLE		MATERIAL G10	Q.A.		
			COMMENTS:		
		FINISH			

Switch Components
G10 tubing and
bottom support plate

Appendix C

LABVIEW Data Acquisition

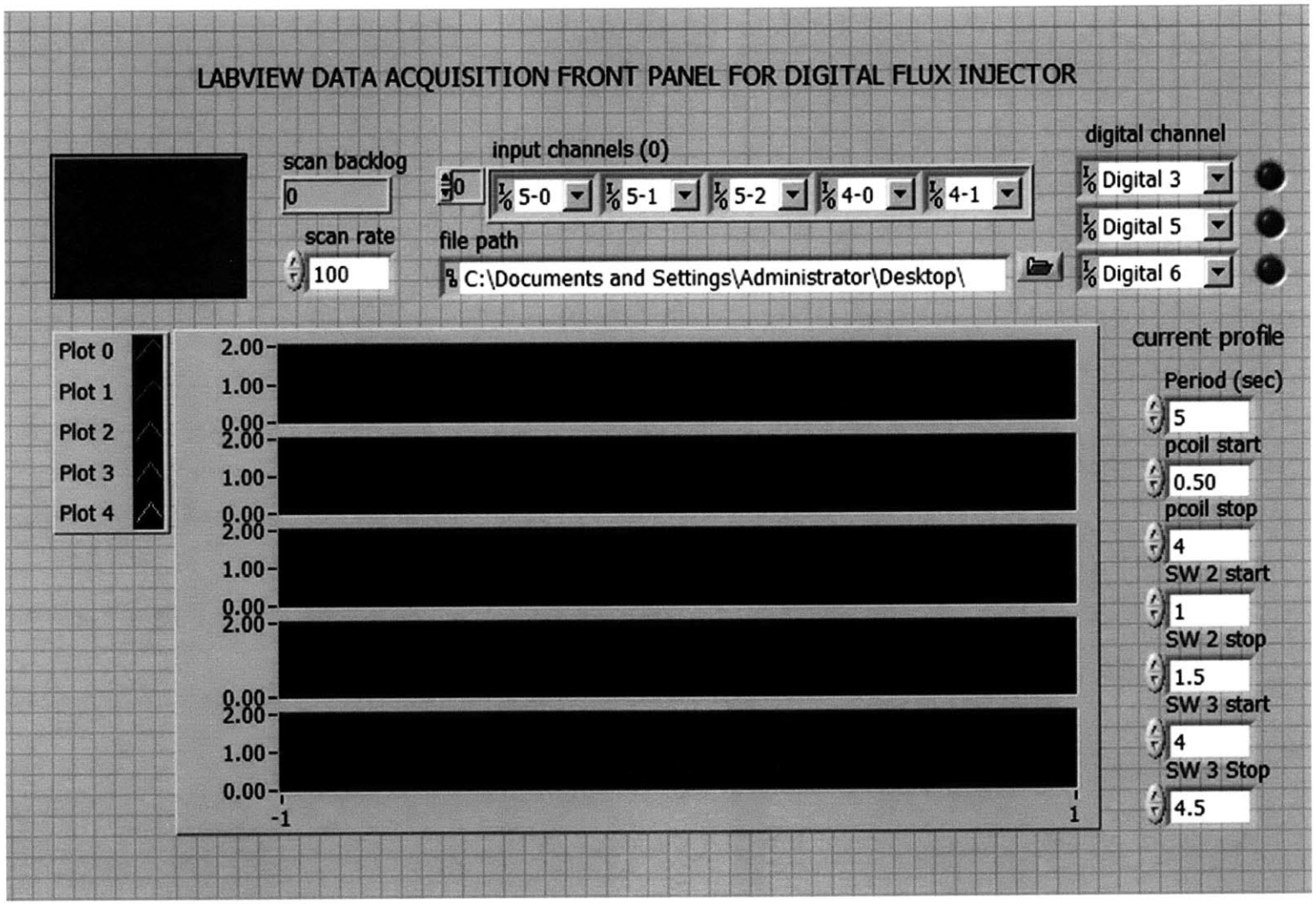
LABVIEW DATA ACQUISITION FRONT PANEL FOR DIGITAL FLUX INJECTOR
scan backlog
0
input channels (0)
0
5-0
5-1
5-2
4-0
4-1
digital channel
Digital 3
Digital 5
Digital 6
scan rate
100
file path
C:\Documents and Settings\Administrator\Desktop\
Plot 0
Plot 1
Plot 2
Plot 3
Plot 4
2.00
1.00
0.00
-1
1
current profile
Period (sec)
5
pcoil start
0.50
pcoil stop
4
SW 2 start
1
SW 2 stop
1.5
SW 3 start
4
SW 3 Stop
4.5

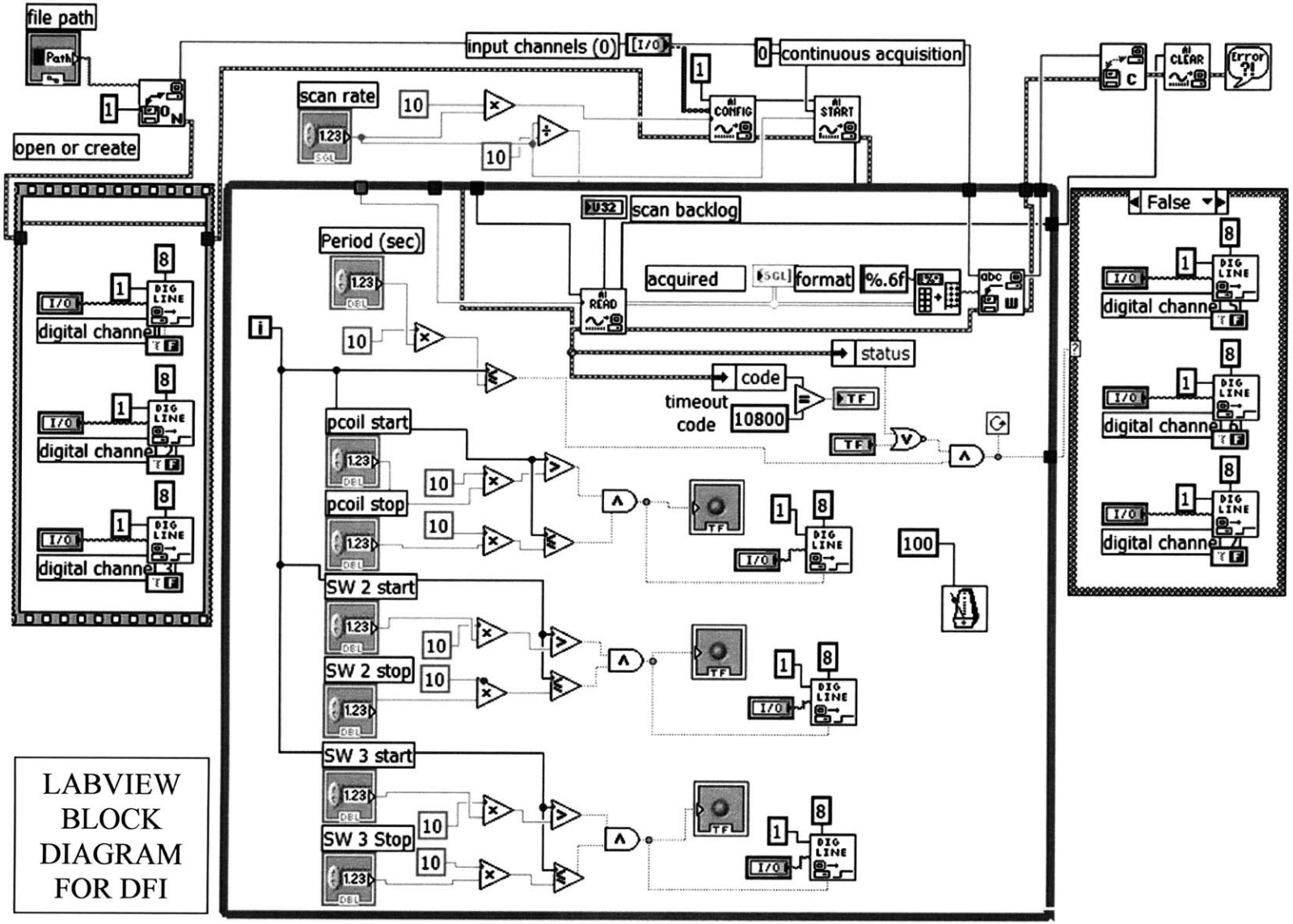

LABVIEW BLOCK DIAGRAM FOR DFI

Appendix D

MATLAB Post-Processing Code

```
% update on 01/14/04
% Flux pump dimensions
% toroid diameter is about 200mm
N_DP = 4; % number of DP, 90deg apart

% GE tape dimension
Thickness = 0.014; % thickness of tape
Width = 0.122; % width of tape

N_pri = 110
N_sec = 6

%normarlly used clearance = 1/8; %clearance, [in]

Cryostat ID = 12.5; %[inch] fixed
Bore OD = 2.75; %[inch] fixed

Baffles OD = 12 + 5/16; % approx value
existing G10 plate OD = 12 + 1/8

% for top/bottom copper plates
OD_plate = 12 inch
ID_plate = 3 inch

% Pancake
delta_R = (OD_plate - ID_plate)/2 = 4.5 inch
   % size of DP G10 plate
L_Gten = delta_R - clearance = 4.375
```

```
   % primary, secondary coils
OD_pri = L_Gten - 2*clearance = = 4.125
ID_pri = OD_pri - N_pri*Thickness = 2.585

glue = 1/16; % inch

OD_sec = ID_pri - glue = 2.523
ID_sec = OD_sec - N_sec*Thickness = 2.439

%*************************************************
OD_pri = 4.125
ID_pri = 2.585
OD_sec = 2.523
ID_sec = 2.439
Width = 0.122

% inputs for sol design program inductance calculation
b = (2*Width+0.040)/2
a1_pri = ID_pri/2
delta_a_pri = (OD_pri-ID_pri)/2
a1_sec = ID_sec/2
delta_a_sec = (OD_sec-ID_sec)/2
```

```
% HTS cryostat volume calculation
%
function volume = volume(z)

% from z = 0 to 19 inch
A1 = pi/4*(12.5^2-5^2+3^2); %sqin

% from z = 19 to 22.5 inch
A2 = pi/4*(12.5^2);

% from z = 22.5 to 23 inch
A3 = pi/4*(12.5^2-10^2);

% from z = 23 to 28 inch
A4 = A2;

if (z<=19)
   volume = A1*z;
elseif (z<=22.5)
```

```
   volume = A1*19+A2*(z-19);
elseif (z<=23)
   volume = A1*19+A2*3.5+A3*(z-22.5);
else
   volume = A1*19+A2*3.5+A3*0.5+A4*(z-23);
end

volume = volume*(2.54^3);
```

```
%This mfile takes input of magnet information bo, B0, Lmg, Iop, Rn and tpp,
% outputs the the performance values of delta iop, delta freq, delta field etc
clc
% LTS Insert Only
bo = 2.08; %1.26; % [T]
Bo = 8.22; %8.22; % [T]
Lmg = 1.55;
%Lmg = 2.66; %1.12; %[H]
Rn = 7e-9; %1500e-9; %[ohm]
tau = Lmg/Rn;

Iop = 75.6; %49; %[A]
tpp = 30; %10 %[s]

Iop_delta = Iop*tpp/tau %[A]

bo_delta = bo*tpp/tau %[T]

%%%%%
drift_rate = 1/tau*bo/Bo*3600e6 %[ppm/h]

avg_freq_band_normalized = 1/2*tpp/tau*bo/Bo*10^6 %[ppm]

delta_freq_normalized = tpp/tau*bo/Bo*10^6 %[ppm]
%%%%%
```

```
%This mfile takes input from performance values calculated in step1.m
% as well as input from inductances to calculate the required current inputs to primary
and secondary coils
```

Lp=1.3475247e-03
Mps=4.2266715e-05
Ls=4.1663732e-06

Lp=0.964e-03
Mps=4.162e-05
Ls=5.03e-06

Lp=Lp*4
Mps=Mps*4
Ls=Ls*4

Ip = Ls/Mps*Iop + (Lmg+Ls)/Mps*Iop_delta %[A]

Is = Iop + (Lmg+Ls)/Ls*Iop_delta %[A]

Lp = 0.0054
Mps = 1.6907e-004
Ls = 1.6665e-005

Lmg = 1.55
Iop = 0

Ip = 8.5
Is = Mps/Ls*Ip

Iop_delta = Ls*(Is-Iop)/(Lmg+Ls)

% defining variables
% conversion factors

Lmg = 0.98; %Henry
Magnet_factor = 0.21; %gauss/mA

Lp = 5.4e-3; %[mH] primary coil, design value
Ls = 0.0167e-3; %[mH] secondary coil, design value
Mps = 0.17e-3; %[mH] mutual inductance, design value

Hall_factor1 = 0.185; %mV/gauss (293k)
% Hall_factor2 = 0.0485; %mV/mA in LTS magnet
Hall_factor3 = 0.217; %mv/gauss (4k)

```
Search_turns = 23540; % number of turns
Search_area = 1.3e-3; % m^2
Search_factor = Search_turns*Search_area;

% Time index is 100th of a second
tpp = 500; % pumping period

first = 1; % first point of data
last = 550000; % approximately last point of pumping

a = 1000; % start for switch temperature profile
b = a+1000; % end for switch temperature

aa = 1; % start for current profiles
bb = 1020; % end for plotting current profiles

% calculating average: start and stop index
c = 300000;
shots = 400;
d = c+shots*tpp; % equals 500000

% plotting pumping shots: start and stop
cc = 399900;
shots2 = 10;
dd = cc+shots2*tpp;
```

```
% processing data
% store measurement data into varibles
% calculations

format short

%thermocouple temperature conversion
p = [7.6e-15, -3.0552e-11, 4.2523e-8, -2.7279e-5, 6.9967e-2, 4.1249];

Time = T; %sec

Pcoil = D; %amp
Heater2 = E;  %amp
Heater3 = F;  %amp
```

```
Temp = G*1000; % becomes microvolt
Temp = polyval(p,Temp); % becomes Kelvin

Volt = M; % mV, voltage across S2

Helium = Q*36; %inch
Helium = Helium*25.4; %mm

ref_vector1 = (1:50);
ref_vector2 = (600000:665000);

Vmg = O ; %mV, magnet terminal voltage
Vmg = Vmg - mean(Vmg(ref_vector1)); % subtract reference value
IntVmg = cumtrapz(Time,Vmg); % integrate over all time
Iop_mg = IntVmg/Lmg; %becomes current, milli-amp
Gauss_mg = Iop_mg*Magnet_factor; % becomes gauss

Vsc = P ;%mV, search coil voltage
Vsc = Vsc - mean(Vsc(ref_vector1)); % subtract reference
IntVsc = cumtrapz(Time,Vsc); % integrate over all time
Gauss_sc = 10*IntVsc/Search_factor; %becomes gauss
%Iop_sc = Gauss_sc/Magnet_factor;

Vprobe = S; %mV
Vprobe = Vprobe - mean(Vprobe(ref_vector1));
Gauss_probe = S/Hall_factor3; %gauss

%Calculations

%%% one shot increment in voltage or integrated voltage
%% Averaging over many shots, use index c and d
oneshot_IntVmg = (IntVmg(d)-IntVmg(c))/shots %mVs per shot
oneshot_IntVsc = (IntVsc(d)-IntVsc(c))/shots %mVs per shot
oneshot_Vprobe = (Vprobe(d) - Vprobe(c))/shots %mV per shot
% oneshot_Iop = (Iop_mg(d)-Iop_mg(c))/shots %mA per shot

%% one shot increment in gauss, averaged from c to d
dGauss_main_magnet = (Gauss_mg(d)-Gauss_mg(c))/shots %gauss per shot
dGauss_search_coil = (Gauss_sc(d)-Gauss_sc(c))/shots %gauss per shot
dGauss_hall_probe = (Gauss_probe(d)-Gauss_probe(c))/shots %gauss per shot

%%% total change in magnetic field density
%% from 1 to 5500 sec, (1100 shots)
Gauss_mg(last)
Gauss_sc(last)
Gauss_probe(last)
```

```
% per shot value, for comparison, average over entire history
dGauss_main_magnet2 = Gauss_mg(last)/1100
dGauss_search_coil2 = Gauss_sc(last)/1100
dGauss_hall_probe2 = Gauss_probe(last)/1100

%% column 1    column 2    column 3   column 4
%% value/shot  avg(c-d)   last value  avg(all)

results = [ oneshot_IntVmg  dGauss_main_magnet  Gauss_mg(last)
dGauss_main_magnet2
        oneshot_IntVsc  dGauss_search_coil  Gauss_sc(last)     dGauss_search_coil2
        oneshot_Vprobe  dGauss_hall_probe   Gauss_probe(last)  dGauss_hall_probe2
        ]

%  theoretical values
Iop = 0;
Ip = 8.64;
Is = Mps/Ls*Ip;

Iop_delta = Ls*(Is-Iop)/(Lmg+Ls); % amp
dIop_expected = Iop_delta*1000;  %mA per shot
dGauss_expected = dIop_expected*Magnet_factor %gauss
```

```
%% plots
%%%%%%%%%%%%%%%%%%%%%%%%%%%%%%%%%%%%%%%%%%%%%%%%%%%%%%%%%%%%%%%%%%%%%%%%%%%%
%%%%%%%%%%%%%%%% Current Profile
FIG0 = figure;
hold on;

%grid on;
%title('Current Profile');

subplot(3,1,1)
plot(Time(aa:bb),Pcoil(aa:bb),'k')
axis([aa/100,bb/100,-2,10]);
xlabel('Time [s]');
ylabel('I [A]');
legend('Primary Coil')

subplot(3,1,2)
plot(Time(aa:bb),Heater2(aa:bb),'k')
```

```
axis([aa/100,bb/100,-2,4]);
xlabel('Time [s]');
ylabel('I [A]');
legend('Switch 2')

subplot(3,1,3)
plot(Time(aa:bb),Heater3(aa:bb),'k')
axis([aa/100,bb/100,-2,4]);
xlabel('Time [s]');
ylabel('I [A]');
legend('Switch 3')

hold off;

%%%%%%%%%%%%%%%%%%%%%%%%%%%%%%%%%%%%%%%%%%%%%%%%%%%%%%%%%%%%%%%%%%%%%%%
%%%%%%%%%%%%%%%%%%% helium level
FIG2 = figure;
hold on;

%grid on;
%title('Helium Level');

plot(Time, Helium, 'k');
xlabel('Time [s]');
ylabel('Helium Level [mm]');
axis([1,6000,600,690]);

hold off;

%%%%%%%%%%%%%%%%%%%%%%%%%%%%%%%%%%%%%%%%%%%%%%%%%%%%%%%%%%%%%%%%%%%%%%%
%%%%%%% %%%%%%%%% switch response
FIG3 = figure;
hold on;

%grid on;
%title('Switch Response');
Ax = plotyy(Time(a:b), Pcoil(a:b), Time(a:b), Temp(a:b))
plot(Time(a:b), Heater2(a:b))
plot(Time(a:b), Vmg(a:b))

legend(Ax(1),'P/Coil Current', 'S2 Current', 'Magnet Insert Voltage',
'Location','NorthWest');

legend(Ax(2),'S2 Temperature');
xlabel('Time [s]')
ylabel(Ax(1), 'I [A]');
```

```
ylabel(Ax(2), 'Temperature [K]');

hold off

%%%%%%%%%%%%%%%%%%%%%%%%%%%%%%%%%%%%%%%%%%%%%%%%%%%%%%%%%%%%%%%%%%%%%%%%
%%%%%%%%%%%%%%%% magnet voltage
FIG4 = figure;
hold on;
%grid on;
%title('Main Magnet Voltage');
subplot(2,1,1)
plot(Time(cc:dd), Vmg(cc:dd),'k')
xlabel('Time [s]');
ylabel('V [mV]');
axis([3999,4050,-2,6]);

subplot(2,1,2)
plot(Time(cc:50:dd), Gauss_mg(cc:50:dd)-Gauss_mg(cc),'k')
xlabel('Time [s]');
ylabel('Bz [gauss]');
%legend('Magnet Voltage Measurement')
axis([3999,4050,0,4]);

hold off;

%%%%%%%%%%%%%%%%%%%%%%%%%%%%%%%%%%%%%%%%%%%%%%%%%%%%%%%%%%%%%%%%%%%%%%%%
%%%%%%%%%%%% search coil voltage
FIG5 = figure;
hold on;
%grid on;
%title('Search Coil Voltage');

subplot(2,1,1)
plot(Time(cc:dd), Vsc(cc:dd),'k')
xlabel('Time [s]');
ylabel('V [mV]');
axis([3999,4050,-2,6]);

subplot(2,1,2)
plot(Time(cc:50:dd), Gauss_sc(cc:50:dd)-Gauss_sc(cc),'k')
xlabel('Time [s]');
ylabel('Bz [gauss]');
%legend('Search Coil Voltage Measurement')
axis([3999,4050,0,4]);

hold off;
```

```
%%%%%%%%%%%%%%%%%%%%%%%%%%%%%%%%
%%%%%%%%%%%%%% hall probe voltage
FIG6 = figure;
hold on;
%grid on;
%title('Hall Probe');

plot(Time(cc:dd), Gauss_probe(cc:dd)-Gauss_probe(cc),'k')
xlabel('Time [s]');
ylabel('Bz [gauss]');
%legend('Hall Probe Voltage Measurement')
axis([3999,4050,0,4]);

hold off;

%%%%%%%%%%%%%%%%%%%%%%%%%%%%%%%%
%%%%%%%%%%%%%%  hall probe long
% FIG7 = figure;
% hold on;
% % grid on;
% %title('Hall Probe');
%
% plot(Time(1:600000),Gauss_probe(1:600000),'k');
%
% xlabel('Time [s]');
% ylabel('Bz [gauss]');

% hold off;

%%%%%%%%%%%%%%%%%%%%%%%%%%%%%%%%
%%%%%%%%%%%% Magnet Current long
FIG8 = figure;
hold on;

plot(Time(1:600000),Iop_mg(1:600000),'k');

xlabel('Time [s]');
ylabel('Iop [mA]');

hold off;

%%%%%%%%%%%%%%%%%%%%%%%%%%%%%%%%
%%%%%%%%%%%%%%%%%%%%%%%%%%%%%%%%
%%%%%%%%%%%%%%%%%%%%%%%%%%
% print -djpeg filename
```

```
% flux pump experiment data processing
% August 2005

clear all
close all
clc
format short
%%%%%%%%%%%%%%%%%%%%%%%%%%%%%%%%%%%%%%%%%%%%%%%%%%%%
%%%%%%%%%%%%%%%%%%%%%%%%%%%%%%%%
%INPUT DATA FILE, STORE IN A MATRIX
cd 'C:\Documents and Settings\Rocky Mai\Desktop\Lab related\new tests\6.sep2005
insert test\raw_day2';
File_in = 'heliumtest4.txt';

M = dlmread(File_in);

%
figure; plot(M(:,1))
%
% figure; plot(M(a:b,1),M(a:b,6))

figure;
plot(M(:,1),M(:,3),'r',...
M(:,1),M(:,4),'y',...
M(:,1),M(:,5),'b',...
M(:,1),M(:,6),'g',...
M(:,1),M(:,7),'k',...
M(:,1),M(:,8),'m',...
M(:,1),M(:,9),'c')
legend('2','3','4','5','6','7','8')

a = find(M(:,1)>20,1,'first')
b = find(M(:,1)>50,1,'first')

% a = find(M(:,1)>,1,'last')
% b = find(M(:,1)>3,1,'last')

for i=2:1:9
s=polyfit(M(a:b,1),M(a:b,i),1);
slope(i-1,:)=s;
end
```

```
slope(:,1)

% scanrate = 100;
% Time = [1:1:size(M,1)]'/scanrate;
% M = [Time,M];
%
% %OUTPUT
% %File_out = 'august\dummy.txt';
% %dlmwrite(File_out,M,'newline','pc')
%
%%%%%%%%%%%%%%%%%%%%%%%%%%%%%%%%%%%%%%%%%%%%%%%%%%%%%%%%%%%%%%%%%%%%%%%%%%%%
%%%%%%%%%%%%%%%%%%%%%%%%%%%%%%%%%%%%%%%%%%%%%%%%%%%%%%%%%%%%%%%%%%%%%%%%%%%%

% %DEFINE CONVERSION FACTORS AND CONSTANTS
% % hall probe conversion
% % #1: 1mA, gain 1000
% % #2: 0.1mA, gain 100
% hp_factor1 = 0.022; %mV per gauss (4K)
% hp_factor2 = 0.0022; %mV per gauss (4K)
% % HTS insert conversion
% hts_factor = 0.25; %gauss per mA (49 DPs)
%
% Lmg = 1; %H
% Lp = 5.4e-3; %[mH] primary coil
% Ls = 0.017e-3; %[H] secondary coil
% Mps = 0.17e-3; %[H] mutual inductance
%
%%%%%%%%%%%%%%%%%%%%%%%%%%%%%%%%%%%%%%%%%%%%%%%%%%%%%%%%%%%%%%%%%%%%%%%%%%%%
%%%%%%%%%%%%%%%%%%%%%%%%%%%%%%%%%%%%%%%%%%%%%%%%%%%%%%%%%%%%%%%%%%%%%%%%%%%%
% %ASSIGN MEASUREMENT DATA TO VARIABLES
% %PLOT VARIABLES VERSUS TIME
%
% % HELIUM LEVEL
% Helium = M(:,5)*36/100; % percentage to inch level
% figure; plot(Time,Helium); legend('Helium');
%
% % TEMPERATURES
% % Type E, reference at between 10 C to 0 C?
% % p2 = [0.0011492, -0.037859, 0.50902, -3.9189, 36.361, 77.323]; % base 77K
% TE = M(:,14);
% figure; plot(Time,TE,'y'); legend ('Type E');
% % thermocouple (gold-chromel) conversion % base 4.2K
% % p = [7.6e-15, -3.0552e-11, 4.2523e-8, -2.7279e-5, 6.9967e-2, 4.1249];
% figure; hold on;
% T1 = M(:,10);
% T2 = M(:,11);
```

```
% T7 = M(:,12);
% T8 = M(:,13);
% subplot(4,1,1); plot(Time,T1,'r'); legend ('SW2 inside');
% subplot(4,1,2); plot(Time,T2,'g'); legend ('SW3 inside');
% subplot(4,1,3); plot(Time,T7,'m'); legend ('Bottom plate');
% subplot(4,1,4); plot(Time,T8,'b'); legend ('Bottom HTS');
% hold off;
%
% %EXTERNAL POWER SUPPLY
% Ich = M(:,9)*4;
% plot(Time,Ich,'b'); legend ('Charging up Current');
%
% %KEPCO PULSES
% Ipc = M(:,6);
% Is2 = M(:,7);
% Is3 = M(:,8);
% figure;
% subplot(3,1,1); plot(Time,Ipc,'b'); legend ('P/coil Current');
% subplot(3,1,2); plot(Time,Is2,'b'); legend ('Sw2 Heat Current');
% subplot(3,1,3); plot(Time,Is3,'b'); legend ('Sw3 Heat Current');
%
% % SWITCHES
% Vs2 = M(:,17);
% Vheat2 = M(:,20);
% Vs3 = M(:,19);
% Vheat3 = M(:,18);
% figure;
% subplot(4,1,1); plot(Time,Vs2,'r'); legend ('SW2 voltage');
% subplot(4,1,2); plot(Time,Vheat2,'g'); legend ('SW2 heat voltage');
% subplot(4,1,3); plot(Time,Vs3,'m'); legend ('SW3 voltage');
% subplot(4,1,4); plot(Time,Vheat3,'b'); legend ('SW3 heat voltage');
%
% % HALL PROBE
% Vhp1 = M(:,15); %mV
% Vhp2 = M(:,16); %mV
% Ghp1 = Vhp1/hp_factor2; % gauss
% Ghp2 = Vhp2/hp_factor2; % gauss
% Ihp1 = Ghp1/hts_factor; % mA
% Ihp2 = Ghp2/hts_factor; % mA
%
% Vhts = M(:,21);
% Ihts = cumtrapz(Time,Vhts)/Lmg;
% Ghts = Ihts*hts_factor;
%
% figure;
% subplot(3,1,1); plot(Time,Ihp1,'b'); legend ('hall probe 1');
```

```
% subplot(3,1,2); plot(Time,Ihp2,'b'); legend ('hall probe 2');
% subplot(3,1,3); plot(Time,Vhts,'b'); legend ('hts insert');
%
%
% % VOLTAGE TAPS
% Vj1 = M(:,22);
% Vj2 = M(:,23);
% Vsp1 = M(:,24);
% Vsp2 = M(:,25);
% Vsp3 = M(:,26);
% Vsp4 = M(:,27);
% Vsp5 = M(:,28);
%
% figure;
% subplot(2,1,1); plot(Time,Vj1,'b'); legend ('joint #1');
% subplot(2,1,2); plot(Time,Vj2,'b'); legend ('joint #2');
%
% figure;
% subplot(5,1,1); plot(Time,Vsp1,'b'); legend ('splice #1');
% subplot(5,1,2); plot(Time,Vsp2,'b'); legend ('splice #2');
% subplot(5,1,3); plot(Time,Vsp3,'b'); legend ('splice #3');
% subplot(5,1,4); plot(Time,Vsp4,'b'); legend ('splice #4');
% subplot(5,1,5); plot(Time,Vsp5,'b'); legend ('splice #5');
%
%
%%%%%%%%%%%%%%%%%%%%%%%%%%%%%%%%%%%%%%%%%%%%%%%%%%%%%%%%%%%%%%%%%%%%%%%%
%%%%%%%%%%%%%%%%%%%%%%%%%%%%%%%%%%%%%%%%%%%%%%%%%%%%%%%%%%%%%%%%%%%%%%%%5
% % INCREASE OR DECAY RATE OF FIELD
%%%%%%%%%%%%%%%%%%%%%%%%%%%%%%%%%%%%%%%%%%%%%%%%%%%%%%%%%%%%%%%%%%%%%%%%
% a=300*100;
% b=700*100;
% m1 = mean(Ihp1(a:b))
% m2 = mean(Ihp2(a:b))
%
% s1 = polyfit(Time(a:b),Ihp1(a:b),1);s1(1)
% s2 = polyfit(Time(a:b),Ihp2(a:b),1);s2(1)
%
% % linear approximation
% figure;hold on
% plot(Time(a:b),Ihp1(a:b),'r'); legend('hallprobe 1')
% plot(Time(a:b),polyval(s1,Time(a:b)))
%
% figure;hold on
% plot(Time(a:b),Ihp2(a:b),'r'); legend('hallprobe 2')
% plot(Time(a:b),polyval(s2,Time(a:b)))
%
```

```
% Reff1 = abs(s1(1)/m1)
% Reff2 = abs(s2(1)/m2)
%
% Iop = abs(m1)/1000, %A
% Ipc = 10;
% period = 5;
%
% dIop = (Mps*Ipc-Ls*Iop)/Lmg*1000/period %% mA/sec
% dGop = dIop*hts_factor %% gauss/sec
```
